nature cell biology

Multi-step pericellular proteolysis controls the transition from individual to collective cancer cell invasion

Katarina Wolf[1], Yi I. Wu[2]†, Yueying Liu[2], Jörg Geiger[3], Eric Tam[4]†, Christopher Overall[4], M. Sharon Stack[2], Peter Friedl[1,5]

Invasive cell migration through tissue barriers requires pericellular remodelling of extracellular matrix (ECM) executed by cell-surface proteases, particularly membrane-type-1 matrix metalloproteinase (MT1-MMP/MMP-14). Using time-resolved multimodal microscopy, we show how invasive HT-1080 fibrosarcoma and MDA-MB-231 breast cancer cells coordinate mechanotransduction and fibrillar collagen remodelling by segregating the anterior force-generating leading edge containing β_1 integrin, MT1-MMP and F-actin from a posterior proteolytic zone executing fibre breakdown. During forward movement, sterically impeding fibres are selectively realigned into microtracks of single-cell calibre. Microtracks become expanded by multiple following cells by means of the large-scale degradation of lateral ECM interfaces, ultimately prompting transition towards collective invasion similar to that *in vivo*. Both ECM track widening and transition to multicellular invasion are dependent on MT1-MMP-mediated collagenolysis, shown by broad-spectrum protease inhibition and RNA interference. Thus, invasive migration and proteolytic ECM remodelling are interdependent processes that control tissue micropatterning and macropatterning and, consequently, individual and collective cell migration.

Cell migration is a fundamental process in early morphogenesis and cancer metastasis that involves a multi-step cascade of coordinated cell adhesion and contractility coupled to proteolytic remodelling of the extracellular matrix (ECM)[1–3]. Multiple sets of proteolytic enzymes, including matrix metalloproteinases (MMP) and serine and cysteine proteases, are upregulated and activated during cancer progression[4–6]. They mediate the chemical and physical modification of the extracellular microenvironment[4,7] by cleaving cell-surface integrins, CD44, growth factors[8] and ECM structural proteins[9,10]. Pericellular proteolysis is spatiotemporally regulated by enzyme processing, enzyme internalization, and the inactivation of the catalytic site by protease-specific inhibitors, such as tissue inhibitor of metalloproteinases (TIMPs)[4,11,12]. Cell-surface proteases are recruited to sites of substrate contact to provide focalized degradation of specific pericellular substrates[3,13,14]. Consequently, adherent cells degrade ECM proteins at focal adhesion and motility structures including lamellae, pseudopodia and invadopodia[15–17]. However, because adhesive contacts and proteolytic cleavage sites are often colocalized, it is unclear how invading cells generate a polarized force towards an extracellular scaffold without compromising mechanotransduction by proteolytic substrate removal.

Invading tumour cells *in vivo* are confronted with three-dimensional (3D) ECM networks that provide physical barriers against the advancing cell body. Fibrillar collagens are mainly processed extracellularly by soluble and membrane-anchored MMPs. MT1-MMP is a key enzyme in fibrillar collagen processing, because genetic deletion leads to severe connective tissue defects[18] and the inability of cells to invade complex 3D extracellular matrices[9,10,19]. Accordingly, migration of proteolysis-competent cells within a 3D matrix leads to small tube-like matrix defects bordered by processed ECM, which is consistent with a protease-mediated decrease in physical ECM resistance[10,13]. However, concepts integrating protease localization and pericellular ECM cleavage into the spatial and temporal context of cell movement within 3D ECM are lacking.

Using dynamic multimodal microscopy we detected protease localization, ECM structure and ECM processing during invasive cell migration through 3D fibrillar collagen. The data provide a time-resolved map of the biochemical and structural consequences of ECM remodelling in the context of cell adhesion, mechanotransduction and cell migration.

[1]Rudolf Virchow Center, DFG Research Center for Experimental Biomedicine and Department of Dermatology, University of Würzburg, Josef-Schneider-Strasse 2, 97080 Würzburg, Germany. [2]Department of Cell & Molecular Biology, Northwestern University Feinberg Medical School, 303 E. Superior Street, Lurie 3-111, Chicago, Illinois 60611, USA. [3]Institute of Clinical Biochemistry and Pathobiochemistry, University of Würzburg, Grombuehlstrasse 12, 97080 Würzburg, Germany. [4]Department of Biochemistry and Molecular Biology, University of British Columbia, Vancouver, British Columbia V6T 1Z3 Canada. †Current addresses: Department of Pharmacology, University of North Carolina, Chapel Hill, North Carolina 27599, USA (Y.I.W.); Department of Protein Engineering, Genentech Inc., 1 DNA Way, South San Francisco, California 94080, USA (E.T.)
[5]Correspondence should be addressed to P.F. (e-mail: peter.fr@mail.uni-wuerzburg.de)

Received 26 April 2007; accepted 21 June 2007; published online 8 July 2007; DOI: 10.1038/ncb1616

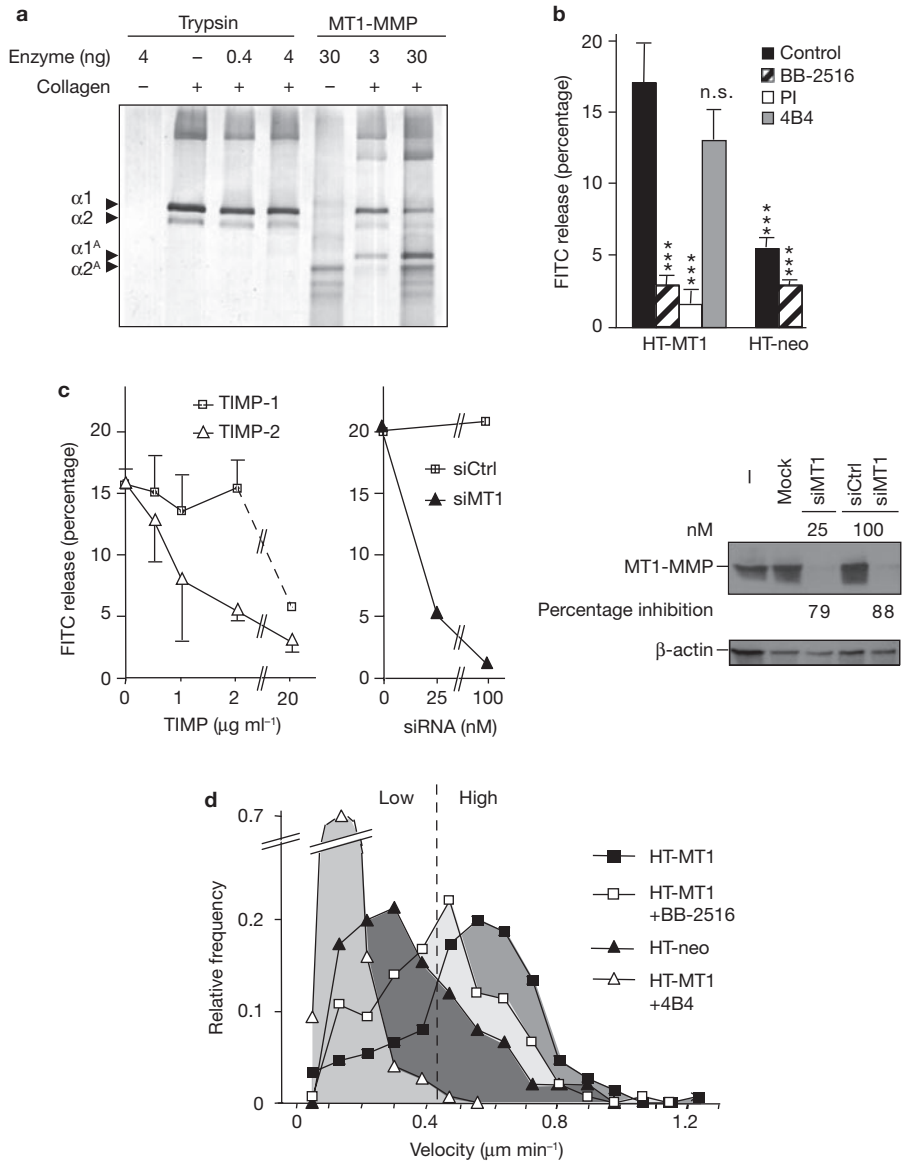

Figure 1 Enhanced collagenolysis and migration of HT-1080 cells in 3D collagen lattices after overexpression of MT1-MMP. (**a**) Dose-dependent collagen degradation by recombinant MT1-MMP but not by trypsin. Full-length chains (α1, α2) and ¾ fragments ($\alpha1^A$, $\alpha2^A$) are indicated. (**b**) Release of soluble FITC from FITC-labelled collagen lattices by HT-MT1 and HTneo cells in the absence or presence of BB-2516 (200 μM), PI cocktail or β_1 integrin function-blocking mAb 4B4 (10 μg ml^{-1}). Results are shown as means and s.d.; $n = 11$. Three asterisks, $P < 0.0001$ compared with untreated HT-MT1 cells (unpaired two-tailed Student's *t*-test). (**c**) Dose-dependent inhibition of collagen degradation from collagen lattices by migrating HT-MT1 cells in the presence of TIMP-2 but not TIMP-1 (means and s.d.; $n = 3$), and after knockdown of MT1-MMP with RNAi. Functionality of TIMP-1 was confirmed at high concentration (20 μg ml^{-1}; $n = 1$) prompting low-affinity interaction between TIMP-1 and MT1-MMP and consecutive inhibition of collagenolysis[21]. MT1-MMP content and β-actin loading control from cell lysates detected by western blot analysis and normalization to β-actin content (decrease in MT1-MMP by 59–79% for 25 nM and 71–88% for 100 nM siMT1). (**d**) Velocity distribution of migrating HT-1080 cells in the presence or absence of BB-2516 (200 μM) or mAb 4B4 (10 μg ml^{-1}). Cells were randomly selected and their mean velocity for a 20-h period was plotted according to frequency in the population ($n = 4$; 160 cells). Population medians (in μm min^{-1}) were 0.64 (HT-MT1), 0.50 (HT-MT1+BB-2516), 0.37 (HT-neo), and 0.15 (HT-MT1+4B4). Categories of 'low' and 'high' velocity separate the respective main peaks of HT-neo and HT-MT1 cells. The percentages within the high-velocity subset were 74% (HT-MT1), 52% (HT-MT1+BB-2516), 31% (HT-neo) and 1% (HT-MT1+4B4). $P < 0.0001$ for all experiments compared with untreated HT-MT1 cells (Kruskal–Wallis test).

RESULTS

MT1-MMP overexpression in HT-1080 cells enhances collagenolysis and migration

To address *in vivo*-like migration within a 3D substrate that provides both adhesion sites and physical resistance towards moving cells, we used non-denatured collagen. The collagen was degraded by MT1-MMP but not by trypsin (Fig. 1a), confirming its native state. Overexpression of MT1-MMP in HT-1080 cells (HT-MT1) cells[20] led to increased MT1-MMP surface levels, the *de novo* appearance of the M_r 43K autolysis product, increased levels of active MMP-2 in zymography (Supplementary Information, Fig. S1), and strongly enhanced degradation of 3D fibrillar collagen (Fig. 1b). These activities were sensitive to the MMP inhibitors GM6001 (ilomastat) and BB-2516 (marimastat) and to a protease inhibitor (PI) cocktail consisting of marimastat,

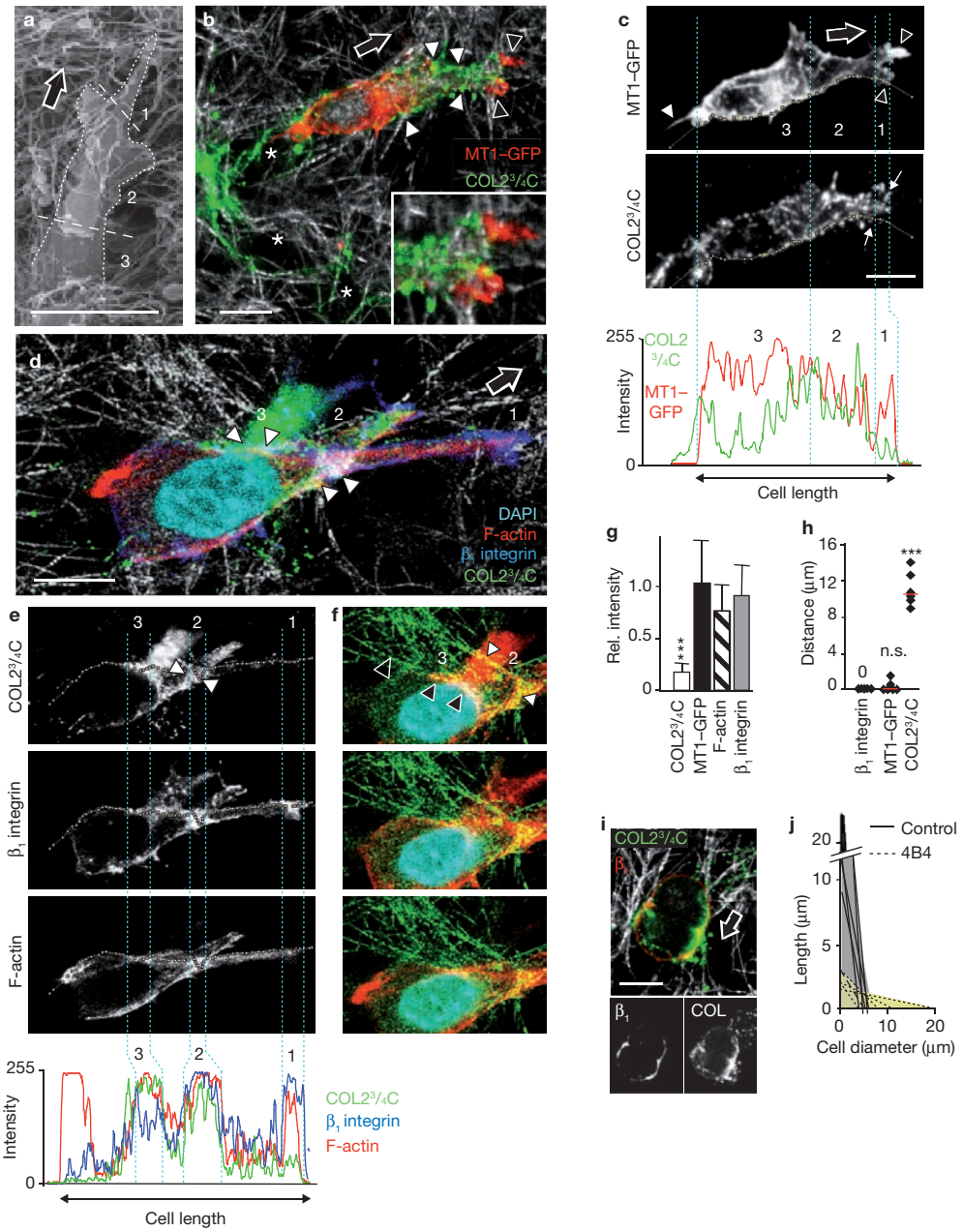

Figure 2 Distinct zones for adhesion, MT1-MMP location and collagenolysis in single migrating cells. (**a**) Definition of morphological zones in migrating HT-1080 cell. Scanning electron micrograph and zones (numbered): 1, leading pseudopod; 2, increasing width; 3, maximum cell diameter. (**b**) Localization of MT1-MMP–GFP (red) and COL2¾C$_{short}$ epitope (green) and physical structure of collagen fibres (grey, reflection). White arrowheads, collagenolysis at contacts to collagen fibres crossing the cell body; black arrowheads, anterior pseudopods rich in MT1-MMP but lacking COL2¾C$_{short}$ epitope; asterisks, track of previous migration. The inset shows a magnification of the leading edge. (**c**) Colocalization analysis from **b**: MT1-MMP–GFP (top), COL2¾C$_{short}$ epitope (middle), and densitometry of pixel intensities along the thin orange lines (bottom). Anterior zone 1 ranged from the tip of the cell (black arrowheads) to the first COL2¾C$_{short}$ peak (white arrows), defining zone 2 thereafter. The white arrowhead indicates a retraction fibre. (**d**–**f**) Segregation of adhesive and proteolytic zones during maximum polarization. (**d**) Maximum-intensity projection of COL2¾C$_{short}$ epitope (green), β_1 integrins (blue), F-actin (red), nuclear DNA (cyan) and collagen (grey; reflection). White arrowheads in **d** and **e** indicate colocalized β_1 integrin, F-actin and COL2¾C$_{short}$ epitope. (**e**, **f**) Colocalization analysis along the thin orange lines (**e**) and colocalization of fluorescence (red pseudocolour) with collagen fibres (green, reflection) (**f**) at pseudopod branches (zone 2, white arrowheads) and at the anterior edge of the nucleus (zone 3, black arrowheads). (**g**) Mean intensities of COL2¾C$_{short}$ epitope, MT1-MMP–GFP, β_1 integrin and F-actin of five cells fixed in a migrating state were normalized to zone 2 as reference and displayed as a mean ratio and s.d. (three asterisks, $P < 0.0001$; unpaired Student's *t*-test). (**h**) Segregation distance of COL2¾C$_{short}$ epitope and MT1-MMP–GFP fluorescence peaks from the anterior tip of the cell, defined by β_1 integrin to the signal ($n = 6$ cells; three asterisks, $P < 0.0001$). (**i**) Loss of cell elongation and polarized segregation of adhesion versus collagenolysis zone in the presence of β_1 integrin function-blocking mAb 4B4. Nonfocalized β_1 integrin (red) and randomly distributed collagenolysis (green) at cell–fibre contacts. (**j**) Pseudopod length until the onset of COL2¾C$_{short}$ epitope (*y* axis) and cell diameter at this site (*x* axis) in the absence or presence of mAb 4B4 ($n = 5$ cells). Black arrows, predicted direction of migration. Scale bars, 10 μm.

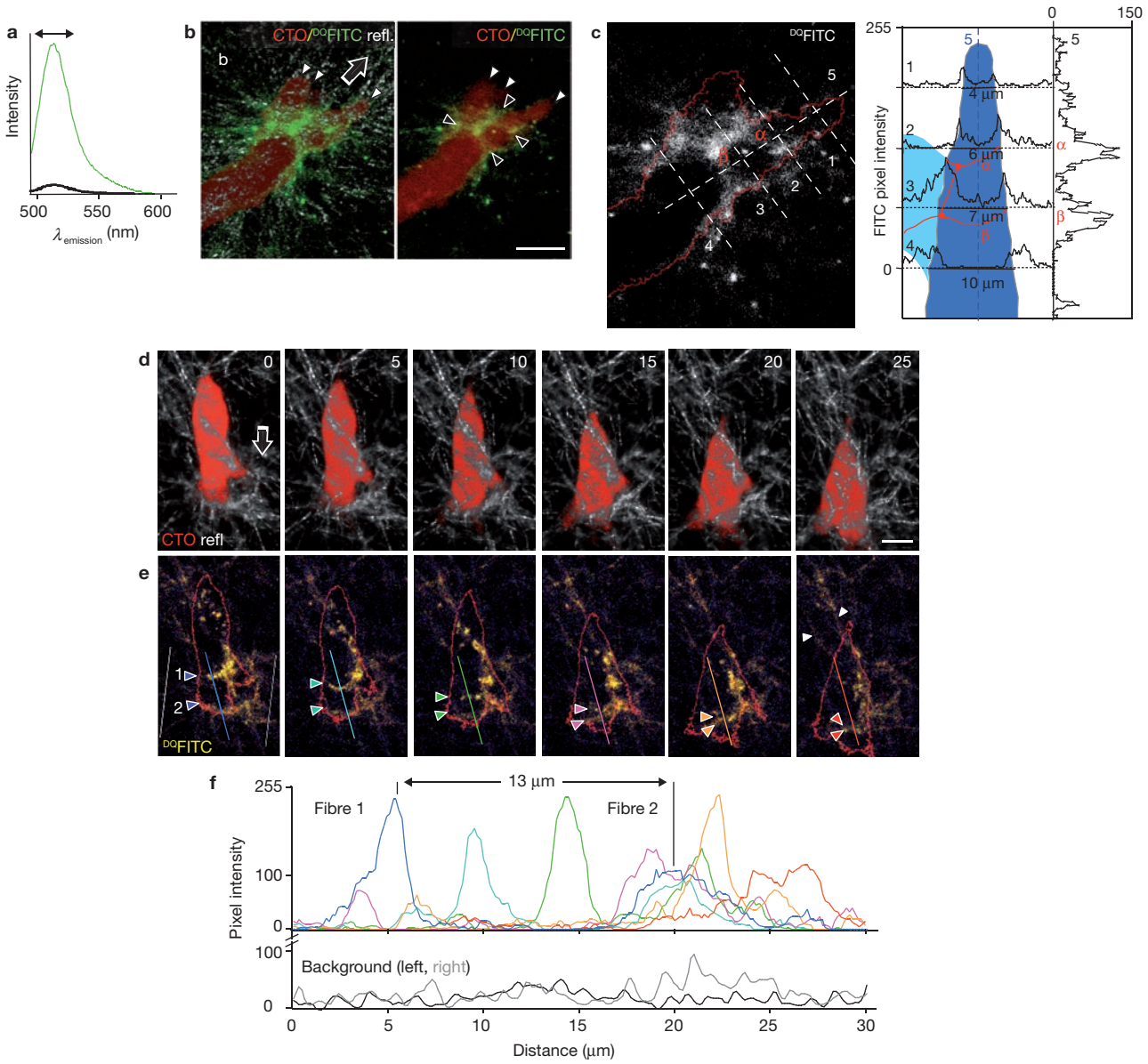

Figure 3 Real-time detection of collagen fibre cleavage and displacement. (**a**) Fluorescence from ^{DQ}FITC-collagen in solution after treatment with collagenase type VII from *Clostridium histolyticum* (green line), compared with a non-treated sample (black line). Arrow, emission range used for confocal microscopy. (**b**) *In situ* dequenching caused by an HT-MT1 cell at the leading edge. Increased fluorescence from ^{DQ}FITC-collagen at collagen fibres crossing cell portions in a belt-like manner (green signal, black arrowheads) and between anterior pseudopod branches (red, CTO). White arrowheads, leading pseudopods and aligned collagen fibres lacking dequenching. (**c**) Reconstruction of ^{DQ}FITC signal of the cell shown in **b** in two axes for the dequenching of lateral (1–4) and perpendicular (5) fibres. Dashed lines mark the tip (1) and the base (2) of the leading pseudopod, pseudopod branching (3) and the final width of the cell body (4). Pixel intensities were obtained along dashed lines (left) and are superimposed on the outline of the cell in blue (right). Two perpendicular fibres (α, β) generating a ^{DQ}FITC signal are marked in red. (**d**–**f**) Collagen fibre cleavage and dislocation in the process of migration. HT-MT1 cell moving within 3D ^{DQ}FITC-containing fibrillar collagen (*z*-projection) shown in Supplementary Information (Movie 2). (**d**) Forward-moving cell body (red) and collagen fibres (grey). Time in minutes is indicated in the top right corner of each frame. (**e**) ^{DQ}FITC signal (yellow) and outline of the cell in **d**. The stepwise transport of two fluorescent fibres (1 and 2) is marked by colour-coded arrowheads and profiles in **f**. White arrowheads indicate dequenched ^{DQ}FITC signal along the track. (**f**) Top: densitometric profile of ^{DQ}FITC signal measured along colour-coded lines in **e**. The peaks corresponding to fibres 1 and 2 changed position in the forward direction until superimposition was reached after 20 min (orange profile). The joint peak moved further in the anterior direction during forward movement (red profile). The dislocation velocity for fibre 1 was 1 µm min^{-1}, as was the migration velocity of the cell in this phase. Bottom: background fluorescence measured adjacent to the cell (grey lines in first frame of **e**). One cell representative of three from independent experiments is shown. Black arrows indicate direction of migration. Scale bars, 10 µm.

trans-epoxysuccinyl-L-leucylamido-(4-guanidino)butane (E-64), pepstatin, aprotinin and leupeptin (Fig. 1b; Supplementary Information, Fig. S1). Collagen degradation by HT-MT1 cells was sensitive to intermediate doses of TIMP-2 but not of TIMP-1, characteristic of MT1-MMP-catalysed collagenolysis (Fig. 1c)[21]. Accordingly, knockdown of MT1-MMP by RNA interference decreased total cellular MT1-MMP protein content by 70–90% and dose-dependently inhibited fluorescein isothiocyanate (FITC) release from 3D collagen lattices (Fig. 1c). Thus, MT1-MMP is rate-limiting in degrading collagen, the loss of which is not compensated for by other collagenases[9,10,19]. Overexpression of MT1-MMP in HT-1080

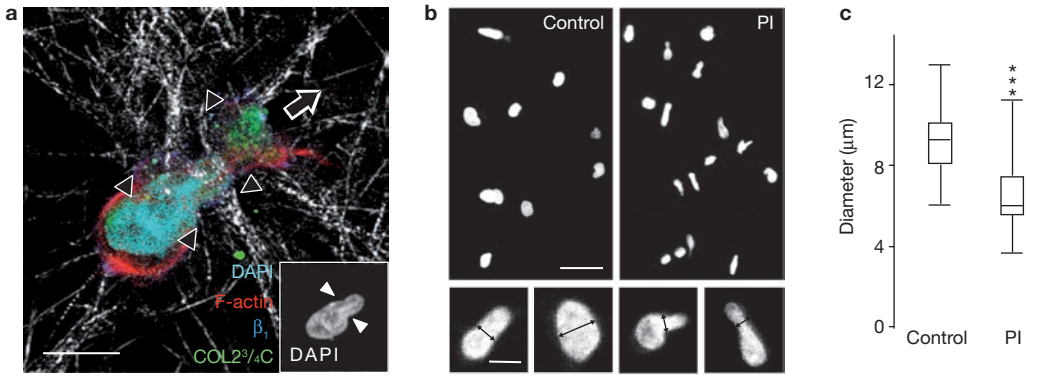

Figure 4 Cell deformation after inhibition of pericellular collagenolysis. HT-MT1 cells maintained migration within 3D fibrillar collagen in the presence of PI cocktail, as shown in Fig. 1d. (**a**) COL2¾C$_{short}$ epitope (green), F-actin (red), β_1 integrins (blue), and nucleus (cyan), showing residual COL2¾C$_{short}$ epitope and cell deformation at locations of perpendicular collagen fibres (arrowheads). The black arrow indicates direction of migration. (**b**) Deformation of nuclei in the absence and presence of PI (*z*-projection of 75 μm depth). (**c**) Nuclear deformation measured as the central diameter as shown by arrows in **b** Three asterisks, $P < 0.0001$, Mann–Whitney *U*-test. Spherical, non-moving or dividing cells detected from the transmission image (not shown) were excluded from analysis. Data represent 50 cells from two independent experiments. Scale bars, 10 μm (**a**, bottom panels in **b**), 50 μm (top panels in **b**).

cells favoured a high-velocity subset (velocity above 0.4 μm min^{-1}), in contrast with neo-vector-transfected control cells (Fig. 1d), which was partly reverted by BB-2516 (Fig. 1d).

HT-1080 fibrosarcoma cells depend on β_1 integrins for mesenchymal-like migration in two-dimensional (2D) and 3D collagen-based models[13,22]. To test whether proteolytic collagen degradation was dependent on integrin-mediated force generation towards collagen fibres and migration, addition of the anti-β_1 integrin function-blocking monoclonal antibody (mAb) 4B4 inhibited cell migration (Fig. 1d)[13] and contraction of collagen matrices (data not shown), but did not substantially decrease collagenolysis (Fig. 1b). Thus, MT1-MMP and β_1 integrins cooperate for proteolytic cell migration but can be functionally uncoupled by antagonizing integrin or protease function, so that both cell functions persist independently.

Focalized cleavage of collagen fibres during migration

To generate a proteolytic map, the leading edge of moving cells was classified into three regions: first, one or few thin anterior pseudopods engaged with collagen fibres; second, the expanding cell body including branched pseudopods; and third, the region of maximum cell diameter (Fig. 2a). For dynamic localization studies, MT1-MMP tagged with green fluorescent protein (GFP) was expressed in HT-1080 cells (HT-MT1–GFP) at low surface levels and confirmed for unperturbed location and function (Supplementary Information, Fig. S1). Most MT1–GFP focalized at pseudopod tips and along the cell body (Fig. 2b,c) with cluster lifetimes of less than 15 min, yet few MT1–GFP clusters persisted for 25 min or longer at fibres crossing the cell body or pseudopod branches, thereby targeting putative physical barriers (Supplementary Information, Fig. S2 and Movie 1). Despite MT1-MMP foci in leading pseudopods, bound collagen fibres lacked a degradation epitope, and only several micrometres back MT1–GFP and the collagen cleavage epitope were colocalized (Fig. 2b, c, zones 1 and 2). Thus, an anterior degradation-free region is followed by a second zone of active collagenolysis. Substantial collagen degradation further localized to the cell rear and along the track of previous migration (Fig. 2b, asterisks).

To achieve a better segregation of the respective locations for matrix adhesion and protease activity, a migratory high-traction phenotype was selected on the basis of the maximum length of leading pseudopods. Whereas the anterior attachment region contained focalized β_1 integrin, MT1-MMP and F-actin but lacked cleavage epitope, posterior zones 8–16 μm distal to the leading edge showed collagen cleavage colocalized with β_1 integrin, F-actin and MT1-MMP (Fig. 2d–h; Supplementary Information, Fig. S3). Cleavage-epitope-positive fibres were bent in a forward direction by pseudopod branches (Fig. 2d, f, white arrowheads) or the nucleus (Fig. 2f, black arrowheads), which is consistent with anterograde pushing. Thus, the front of migrating HT-MT1 cells segregates into an anterior adhesive zone and a posterior proteolytic zone targeting sterically impeding fibres.

To address whether segregation of polarized attachment and collagen cleavage were dependent on the migratory state, cell elongation and force generation were perturbed by using mAb 4B4. With conversion to a partly immobilized round state, the segregation of attachment and proteolysis was abrogated (Fig. 2i, j). Although clustering of β_1 integrin at collagen fibres was lost, pericellular collagenolysis persisted in random locations towards fibres passively touching the cell body (Fig. 2i). Thus, β_1 integrin-mediated traction and cell elongation are required for segregating adhesive from substrate degradation zones, but not for cleaving collagen fibres *per se*.

Invasive MDA-MB-231 breast cancer and wild-type HT-1080 (HTwt) cells not overexpressing MT1-MMP maintained a similar two-zone segregation of lysis-free anterior attachment to several collagen fibres next to posterior collagenolysis (Supplementary Information, Fig. 3). Thus, separate adhesive and proteolytic zones are independent of MT1-MMP overexpression and cell type.

To monitor the steady-state activity of surface collagenases together with the fate of cleaved fibres in real time, fibre processing was measured as dequenched signal emitted from collagen fibres containing dequenchable FITC (^{DQ}FITC). Consequently, collagenase-induced dequenching of ^{DQ}FITC-collagen in solution (Fig. 3a) or from polymerized fibres (Fig. 3b) displayed a strongly increased signal-to-noise ratio (Fig. 3b–f). In moving live cells, peak dequenching was confined almost exclusively to collagen fibres that crossed the cell body in a perpendicular fashion near pseudopod branches (Fig. 3b, black arrowheads) but not pseudopod tips pulling on fibres (Fig. 3b, white arrowheads). Along the length axis, focal dequenching was most prominent at perpendicular fibres that crossed the cell body in a belt-like manner (Fig. 3c, fibres α and β).

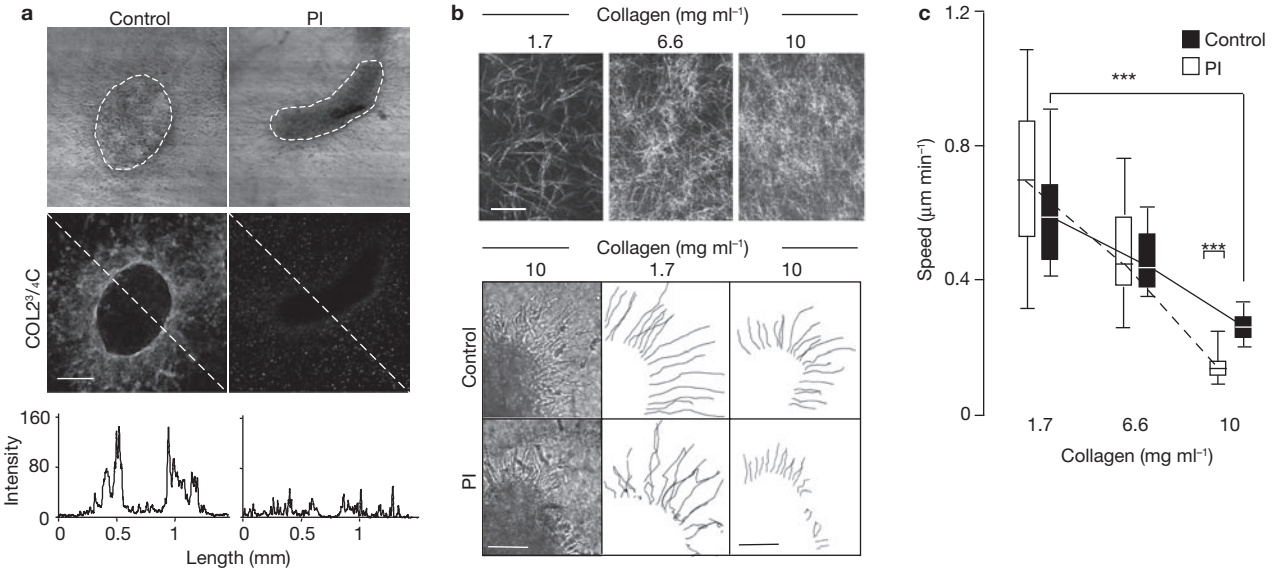

Figure 5 Proteolytic and non-proteolytic migration in high-density collagen spheroid model. (**a**) Detection of collagenolysis by COL2¾C$_{short}$ antibody (middle) at the interface between a multicellular spheroid (dotted line in transmission image (top)) and a collagen lattice after 20 h of culture. The graphs show the relative pixel intensities of COL2¾C$_{short}$ signal along the diagonal lines. (**b**) Fibril structure and density and migration of HT-1080 cells in low-concentration and high-concentration collagen lattices. Top: confocal reflection of low-density and high-density collagen lattices (single scans). Bottom: emigration of HT-MT1 cells from the multicellular spheroids in the absence or presence of PI cocktail. Bottom, left: still images from time-lapse movies (Supplementary Information, Movie 3) after 3.5 h. Bottom, right: migration paths for low-density (1.7 mg ml^{-1}) and high-density (10 mg ml^{-1}) collagen matrices after 5 h of observation. (**c**) Population speed derived from single-cell tracking. Midlines show medians, boxes the 25th and 75th centiles and whiskers the 5th and 95th centiles (20 cells; three asterisks, $P < 0.0001$, non-paired Mann–Whitney *U*-test). Scale bars, 200 μm (**a**), 20 μm (**b**, top), 100 μm (**b**, bottom).

Next, the stepwise opening and dislocation of DQ-signal-intense fibres were detected. Driven by cell movement, loose fibre ends became displaced in a forward direction (Fig. 3d, e, arrowheads; Supplementary Information, Movie 2) and positioned parallel to the cell body (Fig. 3e, f, orange label). Thus, surface-localized collagenolysis leads to the opening of individual fibres, creating loose ends that become realigned in a forward movement direction, thereby forming an oriented scaffold that is apparent after rear retraction (Fig. 3e, white arrowheads).

Blocking fibre cleavage by protease inhibitors causes cell squeezing

To test whether indeed fibres that sterically impede cell movement are cleaved preferentially, proteolytic ECM remodelling was prevented by PI, previously used for the induction of non-proteolytic, amoeboid migration[13]. Treatment with PI abrogated the generation of the COL2¾C$_{short}$ cleavage neo-epitope and enhanced the compression of the cell body and nucleus by perpendicular collagen fibres (Fig. 4a, arrowheads). Compression zones contained focalized MT1-MMP, F-actin and β_1 integrin but not COL2¾C$_{short}$ epitope (Supplementary Information, Fig. S4, white arrowheads), suggesting that PI interfered downstream of the assembly of focal cleavage complexes. In cell populations treated with PI, the median nuclear diameter was decreased by 30% (Fig. 4b, c), which is consistent with fibre-induced physical cell deformation during protease-independent migration.

To address whether collagen removal is the mechanism enhancing migration, we incorporated multicellular spheroids into low-density to high-densitiy collagen matrices mimicking cell evasion from a common origin into dense tissues, similarly to solid tumours. After one day of spheroid culture, a newly formed circular collagen degradation zone of up to 250 μm in diameter was abrogated by treatment with PI (Fig. 5a). In low-density and medium-density collagen (1.7 and 6.6 mg ml^{-1}), control and PI-treated cells had similar migration speeds (Fig. 5b, c), whereas in high-density collagen (10 mg ml^{-1}) protease-competent cells retained a twofold faster migration than that of PI-treated cells (Fig. 5b, c). Thus, despite impaired pericellular collagenolysis and in contrast with data obtained by indirect endpoint migration measures[9,10], time-lapse microscopy reveals sustained migration at 0.1–0.2 μm min^{-1} (Supplementary Information, Movie 3), implicating non-proteolytic movement in low-density and high-density fibrillar collagen.

Essential role of pericellular proteolysis in multicellular invasion

Histopathological sections of different cancers, such as melanoma[23], epithelial cancer[24,25] and sarcoma[26] (Supplementary Information, Fig. S5) typically show quite diverse invasion patterns, ranging from disseminated individual cells to complex 'collective' invasion strands, sheets and clusters[23]. Such multicellular invasion occurs in the absence of epithelial–mesenchymal transition, requires the maintenance of cell–cell contacts[23] and seems to involve MT1-MMP and MMP-2 function[27] and ECM degradation[28]. Using the spheroid invasion model, we therefore tested whether collagen degradation tracks are permissive for the formation of invasive cell strands, as in fibrosarcoma lesions *in vivo*. Initially, tracks generated by an individual 'leader' cell were used by following cells (Fig. 6a–c, asterisks), forming a small cell strand. The matrix defect bordered by proteolytically processed and aligned collagen fibres probably represents paths of least mechanical resistance (Supplementary Information, Movie 4). The diameter of initial tracks reflected the width of individual cells (about 15 μm), whereas tracks

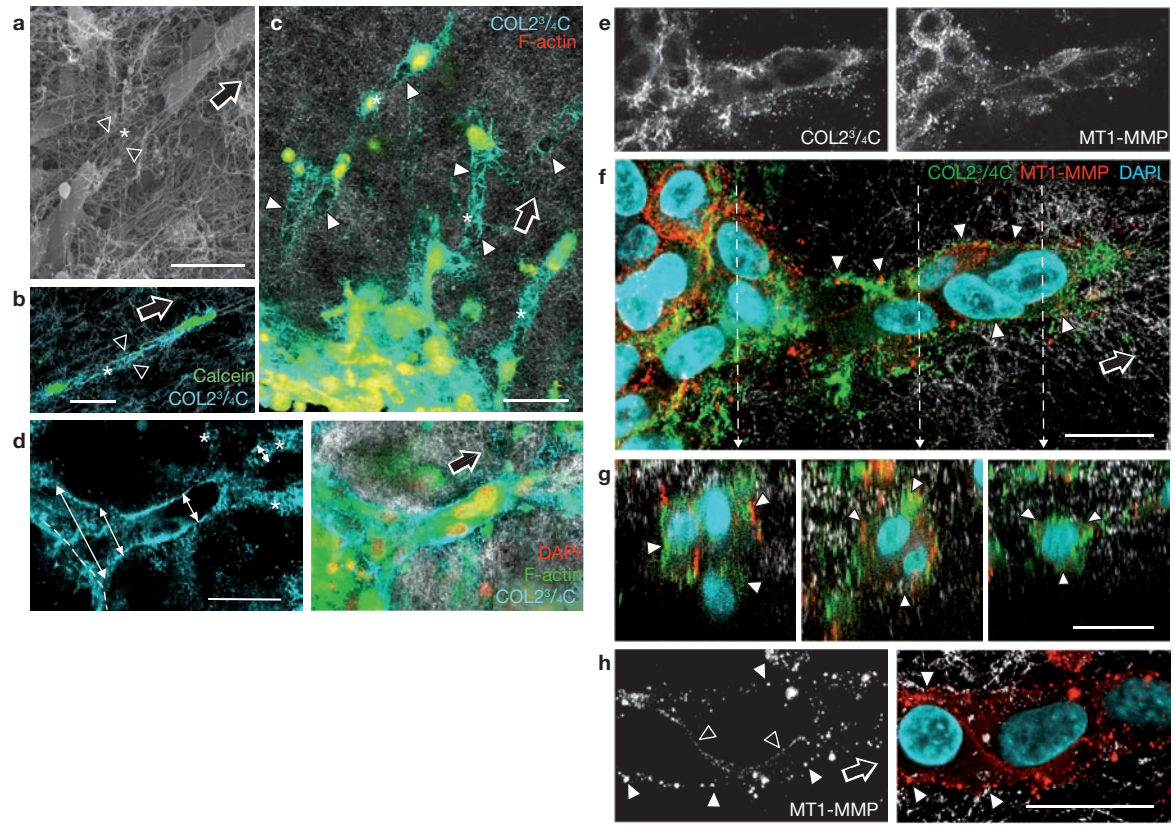

Figure 6 Large-scale removal of ECM layers during multicellular invasion. Invasion of HT-MT1 cells from spheroids into collagen lattices of 3.3 mg ml^{-1} (**a**–**d**) or 6.6 mg ml^{-1} (**e**–**h**) after 20 h of culture. Spheroid locations were in the lower or left position. Staining with calcein-AM (**b**–**d**, green), COL2¾C$_{short}$ antibody (**b**–**d**, cyan; **f**, **g**, green), phalloidin (**c**, red), MT1-MMP (**f**–**h**, red) or DAPI (**d**, red; **f**–**h**, cyan). **a**, **b**, A matrix track (arrowheads) formed by a migrating cell (right) is used by the following cell (left): reconstruction by scanning electron microscopy (**a**) or confocal microscopy (**b**). (**c**) Tube-like matrix defects (arrowheads) lacking inner reflection signal (grey), as reconstructed from a *z*-stack 6 μm thick. (**d**) Diameter expansion of proteolytic paths caused by sequentially migrating cells (*z*-scan and 3D animation in Supplementary Information, Movie 4). White arrows indicate the diameter of the ECM defect determined from the boundary of the COL2¾C$_{short}$ signal, and the dotted line shows the initial boundary of the spheroid. In **a**–**d**, asterisks indicate tracks established by individual cells. (**e**–**g**) Horizontal (**e**, **f**) and vertical (**g**) confocal sections through a multicellular strand and the adjacent ECM, confirming multicellularity and three-dimensionality of the invasion zone (source data and 3D animation in Supplementary Information, Movie 5). White arrowheads indicate patched MT1-MMP (mAb LEM-2/15) associated with the COL2¾C$_{short}$-rich ECM interface. (**h**) Patched and linear distribution of MT1-MMP at cell–ECM (white arrowheads) and cell–cell contacts (black arrowheads), respectively. Black arrows show the direction of migration. Scale bars, 20 μm (**a**, **f**–**h**); 50 μm (**b**–**d**).

filled by subsequent cells increased in calibre (up to 60–80 μm; Fig. 6d) and accommodated up to four cells in juxtaposition (Fig. 6d–g, arrows; Supplementary Information, Movie 4). Notably, with increasing defect diameter, the interface between cells and the collagen scaffold emerged as a near-continuous layer of realigned collagen together with focalized MT1-MMP (Fig. 6d–g; Supplementary Information, Movies 4 and 5), which was consistent with substrate-polarized MT1-MMP engagement towards the adjacent ECM layer. By contrast, MT1-MMP remained evenly distributed along cell–cell junctions within the strands (Fig. 6e–h). Very similar, although less extensive, multicellular invasion strands within expanding collagenolytic tracks were generated by HTwt cells (Supplementary Fig. 6) and MDA-MB-231 cells (Fig. 7), confirming that endogenous collagenase levels were sufficient to support collective invasion[15,29]. Such collective invasion patterns *in vitro* occurred spontaneously, suggesting an inherent programme retained in both mesenchymal HT-1080 and epithelial MDA-MB-231 cells that mimics multicellular strand-like, 'storiform' invasion patterns of fibrosarcoma[26] (Supplementary Information, Fig. S5) and of epithelial masses in ductal breast carcinoma *in vivo*[30].

ECM processing and multicellular strand formation are controlled by MT1-MMP

The importance of proteolytic collagen degradation and transition towards collective invasion was explored with the use of PI treatment. Whereas single-cell migration from spheroids was not affected by PI, collective invasion was abolished (Fig. 7a–c; Supplementary Information, Movie 6). Sustained migration through non-degraded collagen occurred individually or, near the base of the spheroid, as temporary cell doublets, whereas solid multicellular strands within lytic tracks were prevented (Fig. 7b, c, e). Similarly, MDA-MB-231 cells efficiently generated multicellular strands within proteolytic matrix tracks that, again, were abrogated by PI and converted to non-proteolytic single-cell dissemination (Fig. 7d, e).

The transition from collective to single-cell migration was further induced by MT1-MMP knockdown alone, which almost completely prevented collagen degradation (Figs 1c and 8a), lytic track formation and multicellular invasion (Fig. 8b–d). Instead, single-cell migration through non-reorganized collagen was recapitulated (Fig. 8c), which resulted in enhanced morphological adaptation and nuclear deformation (Fig. 8e).

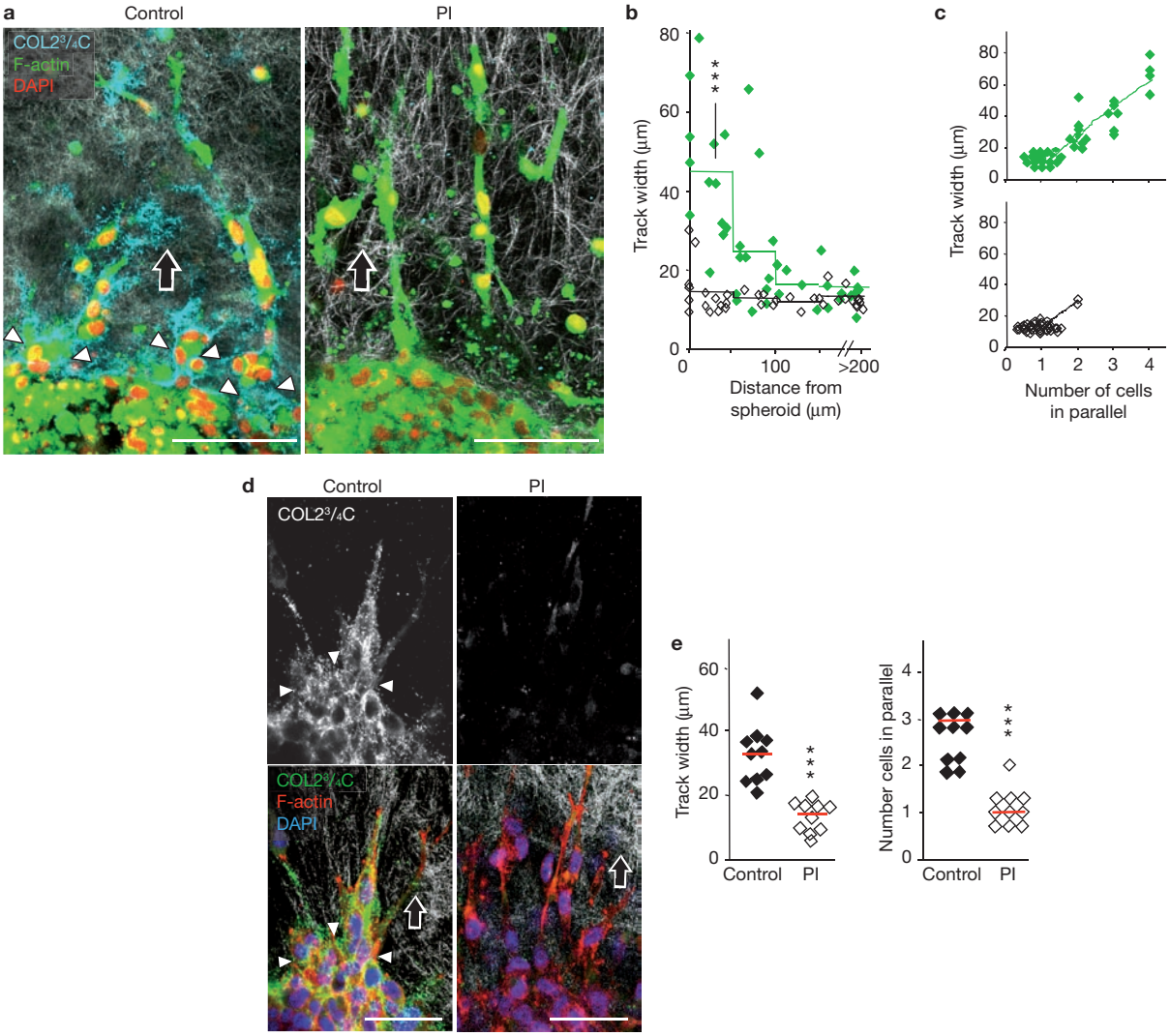

Figure 7 Requirement for pericellular collagenolysis in invasive multicellular but not single-cell migration. Emigration of HT-MT1 (**a**–**c**) and MDA-MD-231 cells (**d**, **e**) from spheroids in the absence or presence of PI cocktail. (**a**, **d**) Abrogation of multicellular proteolytic invasion and persistent non-proteolytic single-cell movement in the presence of PI. White arrowheads indicate collagen degradation zones containing multiple cells. Arrows indicate the direction of migration. (**b**) Abrogation of proteolytic track widening by PI. Data show diameters of cell strands and matrix defects relative to the distance from the spheroid border. Lines represent the means categorized within 50-µm distance intervals from the spheroid margin. Green, control; black, PI. (**c**) Loss of collagenolytic track formation prompts transition from multicellular towards individual cell migration (40 cells, $n = 2$). The endpoints of the slopes represent the diameter of single cells: 15.0 ± 1.16 (control, green) and 13.1 ± 1.65 (PI, black). The correlation coefficient (r) was 0.92 for control cells, confirming a linear dependence of defect calibre and cell positioning in parallel. (**e**) Track widths (left) and number of cells in parallel (right) at 0–50 µm distance from the spheroid in MDA-MB-231 cells in the presence or absence of PI. Three asterisks, $P < 0.0001$, Mann–Whitney U-test for untreated compared with PI-treated cultures (0–50 µm distance range). Scale bars, 100 µm.

The essential function of MT1-MMP in collagen processing and multicellular strand formation was independent of MT1-MMP overexpression, because collective invasion strands, generated by HT-1080 wild-type cells, were suppressed by MT1-MMP knockdown (Supplementary Fig. S6). Taking MT1-MMP overexpression, protease inhibitor treatment or MT1-MMP downmodulation by RNA-mediated interference (RNAi) into context, the formation of collective invasion zones, but not single-cell migration, is a direct function of the cells' capability to degrade collagen and establish lytic tracks (Fig. 8f).

DISCUSSION

Using combined imaging of the cell–matrix interface, MT1-MMP location, physical structure of collagen fibres and the fibre subset undergoing proteolytic degradation, we here identify two modes of pericellular collagenolysis with distinct outcomes: first, the processing of a randomly organized fibrillar collagen network occurs during single-cell migration only at selected regions imposed by belt-like fibres, resulting in fibre reorientation and small tube-like matrix defects; and second, the uniform large-scale clearance of a directly bound ECM layer is achieved by multiple cells that remain connected and cause lateral ECM regression by multicellular invasion. Both proteolytic invasion modes are interconnected and require the function of MT1-MMP: the first type generates ECM micropatterning and facilitates single-cell movement, whereas the second type provides a mechanism for tissue macropatterning by enlarging pre-existing tissue gaps and enabling movement of a tumour mass.

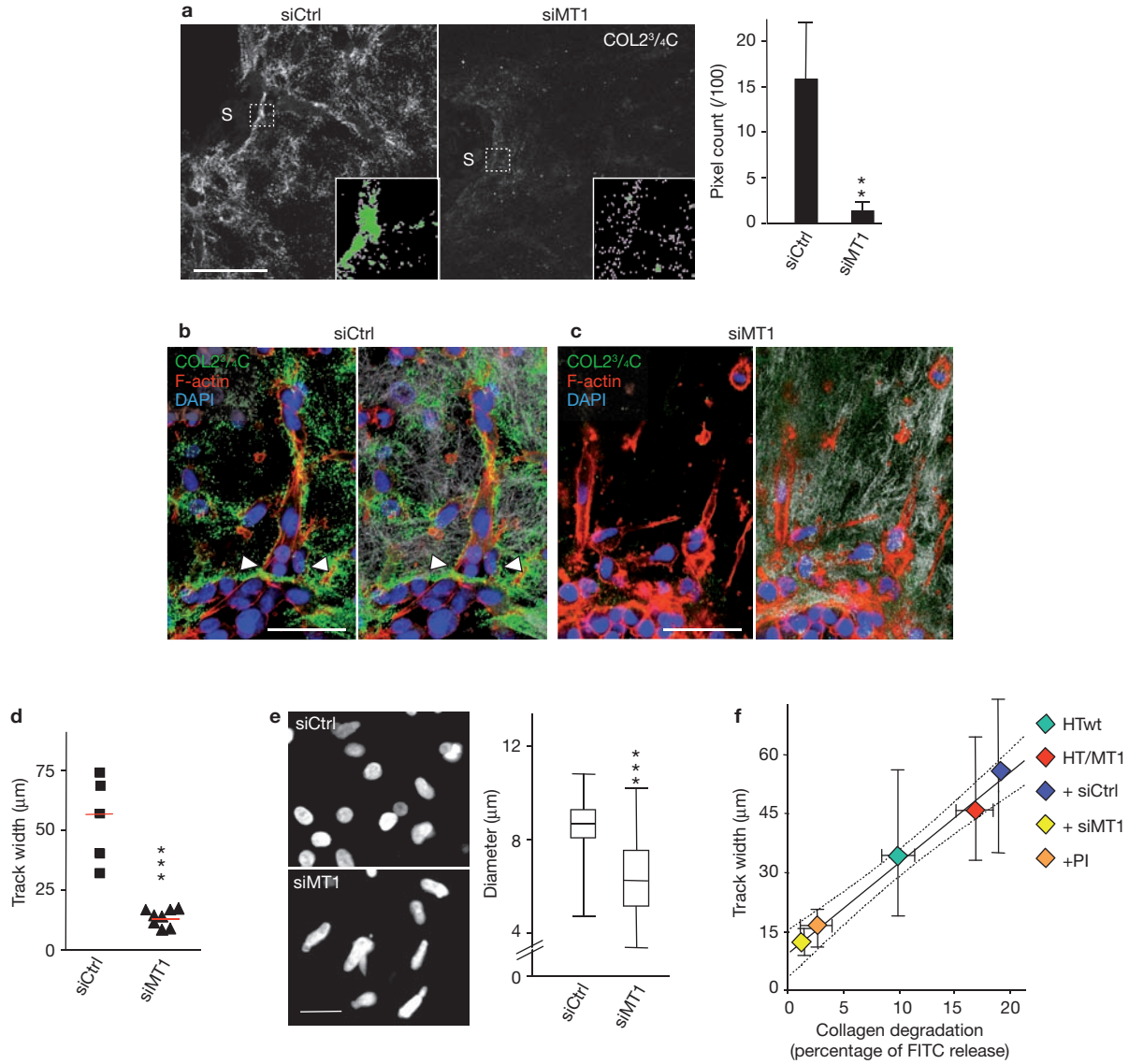

Figure 8 Abrogation of collagenolytic track formation and collective invasion after knockdown of MT1-MMP in HT-MT1 cells. HT-MT1 cells were transfected with 100 nM control or MT1-MMP siRNA and allowed to invade into 3D collagen lattices for 20 h. (**a**) Decrease in collagenolysis adjacent to multicellular spheroids (labelled S). Collagenolytic regions were quantified as pixel count from thresholded images (insets, green false colour) from at least eight different regions (two asterisks, $P = 0.001$, unpaired one-tailed Student's *t*-test). (**b**, **c**) Multicellular collagenolytic track formation (arrowheads) (**b**) and conversion towards single-cell migration (**c**) within collagen matrix lacking cleavage epitope (green); F-actin is shown in red, and nuclei are blue. (**d**) Decrease in track width after MT1-MMP knockdown towards the diameter of single cells near the spheroid–matrix interface. (**e**) Increased nuclear deformation after MT1-MMP knockdown. Spheroid samples were stained with DAPI (left), and the nuclear diameter of single cells after emigration from the spheroids was analysed (right). Three asterisks, $P > 0.0001$, two-tailed Mann–Whitney test. (**f**) Association of multicellular track width with the capability to cleave collagen for different experimental conditions (linear correlation and 95% confidence intervals). Data show medians, maximum and minimum values (track width) and mean values ± s.d. (FITC release from 3D collagen lattices). Correlation was 0.989 with $P = 0.0083$ (Spearman's correlation test). Scale bars, 50 μm (**a**, **b**), 20 μm (**d**).

Time-resolved topographic analysis permits the integration of proteolytic ECM remodelling into known physicochemical steps of cell migration[31,32]. First, the gain of cell polarity by pseudopod protrusion along an ECM scaffold occurs independently of substrate degradation. Second, along protruding pseudopods, both MT1-MMP and β_1 integrins colocalize at actin-rich cell–matrix interaction sites. Integrins transmit adhesive traction force and pull collagen fibres towards the cell body, yet short-lived MT1-MMP patches at collagen fibres lack signs of enzymatic degradation. Third, as the cell glides forward, those collagen fibres that impose steric constraints become focally cleaved, generating loose fibre ends. Three-dimensional and four-dimensional imaging of fibre impressions into the cell body suggests two types of physical resistance: perpendicular fibres that insert between and separate pseudopod branches, and circumferential belts constraining the nucleus. Fourth, disconnected fibre ends remain bound to and become relocated with the moving cell body in the forward direction. Last, rear-end retraction of the cell reveals the migration track of aligned fibres bordering an inner region cleared of ECM. Thus, sequential steps of pericellular proteolysis mediate ECM remodelling during distinct phases of the migration cycle[3,13,33].

In 2D models, integrins and proteases including MT1-MMP colocalize with ECM degradation at outward lamellae and invadopod-like structures underneath the cell[15,16,27,34]. By contrast, if confronted with 3D tissue barriers, the leading edge of moving cells develops at least two subregions: an anterior adhesive zone and a posterior proteolytic zone. Thus, although rich in MT1-MMP, anterior sites providing attachment and force generation seem protected from premature substrate loss. Similar zonal segregation during 3D cell movement is known for anterior Rac-dependent ruffle formation coupled to an adjacent contractile zone controlled by Rho/ROCK[35]. Similarly, spreading osteoclasts produce an anterior actin-rich lamella, termed the sealing zone, and a posterior region of proteolysis towards the bone substrate[36]. Thus, segregating adhesion from substrate processing regions might permit the simultaneous execution but spatial separation of potentially confounding cell functions.

The topographic control mechanism of pericellular proteolysis at submicrometre resolution is unknown. It is established that integrin-mediated signals enhance the expression, focalization to substrate and activity of MT1-MMP and other MMPs[14]. However, MT1-MMP does not interact directly with β_1 or β_3 integrins, as is shown by the lack of coimmunoprecipitation[17,37], and there is a lack of direct evidence for MT1-MMP binding to cytoskeletal proteins. Instead, MT1-MMP binds multimeric substrate, such as a collagen fibre, by its haemopexin C domain[38], possibly favouring substrate-induced MT1-MMP retention and clustering. Thus, extracellular regulation based on substrate proximity and duration of substrate interaction could control local MT1-MMP activity as well as diffusion access of endogenous inhibitors, such as TIMPs[39].

In 3D collagen lattices, the proteolytic remodelling of collagen fibres comprises a topographic physical component not addressed by classical models for measuring protease activity. In biochemical assays collagen is cleaved by MT1-MMP and other collagenases and is further disintegrated to low-molecular-mass fragments by gelatinases[38]. In cell-based 2D substrate degradation assays, almost total removal of collagen or gelatin substrate occurs underneath a migrating cell[16,27]. In 3D fibrillar ECM, however, individual fibres have multiple proteolytic foci but eventually become clipped at a single site, thereby creating loose ends that are realigned and 'recycled' during forward movement rather than dissolved. Although described here for cancer cells, focal fibre cleavage and realignment to ordered strands may represent a fundamental process in ECM micropatterning by other cell types, including activated stroma cells that reorganize provisional matrix during morphogenesis and tissue repair[40,41].

MT1-MMP promotes cell migration in 2D and 3D migration models[9,10,34] by different mechanisms, including adhesion receptor and growth factor processing[8], enhanced focal contact turnover and extracellular signal-regulated kinase activation[42]. MT1-MMP is further rate-limiting in extracellular or intracellular collagen degradation and remodelling and is considered to be a key regulator of matrix density and ECM barrier function[10,13,19]. It remains controversial whether pericellular proteolysis is indispensable for migration in 3D ECM and how fibre structure and spacing determine the protease dependence of cell movement[3,10]. In fibrillar collagen-based ECM comprising sufficient gaps and spaces *in vitro* and *in vivo*, abrogation of protease function prompts rescue of migration by enhanced shape change coupled to actomyosin dynamics[13,35,43]. Conversely, in high-density non-fibrillar ECM including reconstituted basement membrane lacking discrete gaps, the abrogation of proteolytic activity impairs cell migration more stringently[9,44,45]. Consistent with the physical-spacing model, high-density fibrillar collagen counteracts collagenase-independent migration but fails to induce migration arrest. Consequently, physically constraining fibres cause increased compression of both cell body and nucleus, and support shape change as a mechanism for sustaining non-proteolytic migration[13]. Thus, rather than acting as a prerequisite for cell migration, proteolytic tissue micropatterning is secondary to single-cell movement yet its auxiliary function is proportional to ECM density.

Multicellular invasion contributes to morphogenesis and regeneration, but also to cancer invasion[23,27,46,47]. The invasive edge of fibrosarcoma lesions and ductal breast carcinoma *in vivo* commonly develops multicellular strands alongside patterned ECM[26,30]; these strands are similar to strands developing from HT-1080 and MDA-MB-231 cell spheroids. In contrast with tissue micropatterns formed by single cells, collective cell strands measure up to several cell diameters and therefore require removal of the ECM barrier, in a similar manner to protease-dependent vascular sprouting[3,48]. Focalized MT1-MMP along the edge of moving cell collectives generates a continuous proteolytic 2D interface layer towards fibrillar collagen, a process partly mimicked by 2D substrate degradation assays *in vitro*[16,27]. The proteolytic interphase then undergoes structural outward modification, which is equally sensitive to broad-spectrum protease inhibition and interference with MT1-MMP. Thus, MT1-MMP is the key enzyme in the proteolytic macropatterning of collagen-rich ECM to generate space for the cell masses. The process of ECM regression in response to an expanding cell compartment is consistent with the MMP dependence of many cancers during progression[5,6,19] and may explain the as yet poorly understood tissue dynamics that shift cell and ECM interfaces during collective invasion, invasive growth or even expansive growth in the absence of active invasion. Although cell migration and pericellular proteolysis can be dissociated and may continue independently, both processes provide a concurrent, spatially controlled and synchronized contribution to the overall invasion process, and if coupled they are indispensable for the formation of cell and tissue patterns. □

METHODS

Cells, antibodies and inhibitors. The following cell lines were used: human HT-1080 fibrosarcoma cells transfected with MT1-MMP (HT-MT1) or neomycin vector (HT-neo)[20], provided by E. Deryugina and A. Strongin; wild-type HT-1080 cells (HTwt) (ACC 315; DSMZ Braunschweig, Germany); HT-1080 cells transfected with MT1-MMP C-terminally fused to membrane-targeted enhanced green fluorescent protein (mEGFP) (MT1–GFP) using a modified mEGFP–N1 vector (Clontech); mock-transfected HT-1080 cells expressing mEGFP–N1 (N1–GFP) vector alone; and human wild-type MDA-MB-231 breast carcinoma cells. After transfection, cells were controlled for MT1–GFP surface localization, focalization to collagen fibres, autolytic degradation to the M_r 43K cleavage product, increased MMP-2 activation, and promotion of increased migration rates (Supplementary Information, Fig. S1). All cells were cultured in Dulbecco's modified Eagle's medium (PAN), 50 U ml^{-1} penicillin and 50 µg ml^{-1} streptomycin (PAN), 10% heat-inactivated fetal calf serum (FCS; Biowhittaker) and, when transfected, 0.2 mg ml^{-1} G418 (Oncogene) at 37 °C and 5% CO_2 in a humidified atmosphere. Multicellular spheroids were obtained after 24 h of culture in low-adhesive culture dishes (Nunc).

The following antibodies were used: rabbit polyclonal anti-MT1-MMP IgG recognizing the hinge region (Ab815; Chemicon); mouse monoclonal anti-MT1-MMP IgG recognizing the catalytic region (clone LEM-2/15; Chemicon); mouse monoclonal anti-β_1 integrin IgG_1 and IgG_{2a} (clones 4B4 and K20; Coulter-Immunotech); polyclonal chicken anti-human β-actin (Abcam), rabbit polyclonal COL2¾C_{short} IgG (IBEX Pharmaceuticals) raised against a peptide homologous

to the C terminus of the primary cleavage site on type II collagen[49]. Antibody COL2¾C$_{short}$ cross-reacts with the C-terminal Gly 775-Leu/Ile 776 neo-epitope of type I collagen α1 and α2 chains after cleavage by collagenases[49]. Further, isotypic mouse or rabbit IgGs (Dianova) and secondary Alexa-488-conjugated, Alexa-568-conjugated or Alexa-647-conjugated preabsorbed goat anti-mouse or anti-rabbit IgG or F(ab′)$_2$ fragments (Molecular Probes) were used. Protease inhibitors were as follows: broad-spectrum MMP inhibitors GM6001 (ilomastat, Chemicon) or BB-2516 (marimastat; British Biotech); protease inhibitor (PI) cocktail including marimastat (50 μM), pepstatin A (50 μM; Sigma), E-64 (50 μM; Sigma), aprotinin (0.7 μM; Sigma) and leupeptin (2 μM; Molecular Probes); and recombinant TIMP-1 and TIMP-2 (provided by R. Fridman)[12]. All were used at a non-cytotoxic concentration[13].

Knockdown of MT1-MMP by RNAi. A mixture of four small interfering RNAs (on-target *plus* short interfering RNA (siRNA) pool; Dharmacon) against human MT1-MMP (siMT1; forward, 5′-GGAUGGACACGGAGAAUUUUU-3′, 5′-GGAAACAAGUACUACCGUUUU-3′, 5′-GGUCUCAAAUGGCAACAUAUU-3′, 5′-GAUCAAGGCCAAUGUUCGAUU-3′) or control RNAs non-targeting the human, mouse or rat genome (siCtrl; forward, 5′-UGGUUUACAUGUCGACUAA-3′, 5′-UGGUUUACAUGUUGUGUGA-3′, 5′-UGGUUUACAUGUUUUCUGA-3′, 5′-UGGUUUACAUGUUUUCCUA-3′; Dharmacon) were transferred into HT-MT1 or HTwt cells with Dharmafect 4 reagent in accordance with the manufacturer's protocol. Transfection efficiency was at least 90%, as monitored by transfection with a fluorescent probe (OPTI-Green siRNA) and flow cytometry. Maximum downregulation of MT1-MMP protein was obtained after 20 h and persisted for up to 72 h. MT1-MMP knockdown efficiency was determined by western blot analysis (detection antibody LEM2/15) from whole-cell lysates and densitometric analysis. After transfection, cells were cultured for 20 h, detached by EDTA and used for function studies. Toxicity of the interference protocol was excluded on the basis of intact migration function and the lack of membrane damage detected by staining with propidium iodide (Sigma) and flow cytometry.

Cell culture in 3D collagen lattices. 3D collagen matrix cultures were prepared as described[13] with the use of pepsinized dermal bovine collagen (Vitrogen; Nutacon). Individualized cells from subconfluent cultures after detachment by EDTA (2 mM) or multicellular spheroids were incorporated into collagen solution (1.7 mg ml^{-1}) at physiological pH (ref. 13). To generate collagen lattices of 3.3, 6.6 or 10 mg ml^{-1}, high-density acidic stock solution (10–15 mg ml^{-1}) was generated by partial evaporation (Speed Vac; Eppendorf). After polymerization of the collagen lattice, FCS-containing medium (6% final FCS concentration) was added as supernatant. Because of a better-defined fibrillar structure for structural imaging (confocal reflection), most experiments were performed with pepsin-digested collagen and confirmed with non-pepsinized collagen.

Collagen degradation assays. The native state of the type I collagen used as a migration substrate was confirmed by enzymatic *in vitro* degradation[38]. Buffered collagen solution was incubated with trypsin or recombinant MT1-MMP (provided by British Biotech Pharmaceuticals) activated by 4-aminophenylmercuric acetate (18 h, 28 °C), subjected to SDS–PAGE (7.5%) under non-reducing conditions and revealed by staining with silver nitrate.

The degradation of fibrillar collagen by migrating cells was obtained as fluorescence released from collagen lattices containing ^{DQ}FITC-labelled type I collagen monomers (2%; Molecular Probes)[13]. After 40 h of culture, solid-phase collagen including cells was pelleted, and the supernatant containing released FITC-collagen fragments was analysed spectrofluorimetrically (Luminescence Spectrometer LS50; Perkin-Elmer).

The subcellular localization of collagen degradation by live cells during migration was analysed by using collagen lattices containing 5% ^{DQ}FITC collagen[43]. The signal-to-noise ratio was controlled by spectrofluorimetry with excitation at 490 nm by using monomeric ^{DQ}FITC-collagen in PBS (5 μg ml^{-1}) in the presence or absence of type VII collagenase from *Clostridium histolyticum* (7 U ml^{-1}; 1 h, 37 °C). The specificity of ^{DQ}FITC signal from fibrillar collagen detected by confocal microscopy was confirmed by negligible background signal under different conditions, including the following: cell-free lattices; cell-adjacent positions; pseudopod tips generating maximum traction towards collagen fibres, excluding the mechanical unmasking of cleavage epitope; cell-containing lattices in the presence of PI; and collagen matrices containing non-proteolytic T cells[43].

Time-lapse microscopy and quantification of cell migration. Individual cells or multicellular spheroids incorporated within 3D collagen matrices were monitored by digital bright-field microscopy (37 °C, 20 h)[13]. Cell viability after 24 and 48 h of culture in collagen in the presence of antibodies or inhibitors was routinely monitored after digestion with collagenase followed by propidium iodide staining and flow cytometry[13]. Migration was quantified by computer-assisted cell tracking of randomly selected cells, using the *xy* coordinates of cell paths (12-min step interval)[13]. The speed was calculated as the length of each cell path divided by time. The steady-state velocity excludes stopping phases and represents the mean individual step length exceeding the pixel resolution of 1.2 μm (corresponding to 0.1 μm min^{-1}). Statistical analysis was obtained from the two-tailed unpaired Student's *t*-test or the two-tailed unpaired Mann–Whitney test or Kruskal–Wallis test.

Confocal and scanning electron microscopy and image analysis. Cell-containing collagen lattices were cultured for 9–20 h and incubated with calcein acetoxymethyl ester for 1 h at 37 °C, washed and fixed with 4% buffered paraformaldehyde (37 °C, 30 min), stained with the primary and secondary antibodies phalloidin-Alexa568 (Molecular Probes) and 4,6-diamidino-2-phenylindole (DAPI; Roche Diagnostics) for three-dimensional reconstruction by confocal microscopy (Leica-SP2 scanner)[13]. For dynamic imaging of collagen cleavage and fibre remodelling in live samples, cells were labelled by Cell Tracker Orange (CTO; 1 μM; Molecular Probes), incorporated into ^{DQ}FITC-containing collagen lattices and monitored at 5 min time intervals for *z*-reconstruction of cell morphology (transmission, CTO channel), reflection (fibrillar structures) and FITC fluorescence (dequenching during proteolysis). Pixel intensity analysis was performed from individual eight-bit channels or maximum-intensity projections from *z*-stacks (ImageJ 1.30v; W. Rasband). The nuclear diameter was calculated from *z*-projections at either central position or, for irregular shapes, the centre of the deformation zone. For scanning electron microscopy, tumour spheroids were cultured in 3D fibrillar collagen for 20 h, fixed by glutaraldehyde (2.5%), dehydrated stepwise with ethanol (30–100%), and dried in the presence of hexamethyldisilazane (100%). Samples were spattered with platinum and scanned (DSM 962; Zeiss).

Note: Supplementary Information is available on the Nature Cell Biology website.

ACKNOWLEDGEMENTS

We thank M. Ott, M. Kuhn and A. Staudigel for excellent technical assistance; L. King for supplying COL2¾C$_{short}$ antibody; British Biotech Inc., UK, for supplying BB-2516; R. Fridman for supplying recombinant TIMP-1 and TIMP-2; E. Deryugina and A. Y. Strongin for providing HT-1080 cell lines; D. Pei for supplying human MT1-MMP cDNA; K. Müller-Hermelink for providing access to the confocal facility; and G. Krohne for providing access to electron microscopy. This work was supported by the Deutsche Forschungsgemeinschaft (FR 1155/7-1) and Deutsche Krebshilfe (AZ 106950). C.O. was supported by a Canada Research Chair Grant in Metalloproteinase Proteomics and Systems Biology, and E.T. by a CIHR Cell Signals Training Grant. S.S., Y.W. and Y.L. were supported by a research grant from NIH (RO1 CA86984).

AUTHOR CONTRIBUTIONS

P.F. and K.W. conceived and designed the experiments. K.W., Y.W., Y.L. and E.T. performed the experiments. K.W., P.F. and J.G. analysed the data. S.S., J.G. and C.O. contributed reagents, material and analysis tools. K.W. and P.F. wrote the paper. All authors read and corrected the manuscript.

COMPETING FINANCIAL INTERESTS

The authors declare no competing financial interests.

Published online at http://www.nature.com/naturecellbiology/
Reprints and permissions information is available online at http://npg.nature.com/reprintsandpermissions/

1. Stetler-Stevenson, W. G., Liotta, L. A. & Kleiner, D. E. Jr. Extracellular matrix 6: role of matrix metalloproteinases in tumor invasion and metastasis. *FASEB J.* **7,** 1434–1441 (1993).
2. Palecek, S. P., Loftus, J. C., Ginsberg, M. H., Lauffenburger, D. A. & Horwitz, A. F. Integrin-ligand binding properties govern cell migration speed through cell–substratum adhesiveness. *Nature* **385,** 537–540 (1997).
3. Friedl, P. & Wolf, K. Tumour-cell invasion and migration: diversity and escape mechanisms. *Nature Rev. Cancer* **3,** 362–374 (2003).
4. Sternlicht, M. D. & Werb, Z. How matrix metalloproteinases regulate cell behavior. *Annu. Rev. Cell Dev. Biol.* 17,463–516 (2001).

5. Coussens, L. M., Fingleton, B. & Matrisian, L. M. Matrix metalloproteinase inhibitors and cancer: trials and tribulations. *Science* **295,** 2387–2392 (2002).
6. Zhai, Y. *et al.* Expression of membrane type 1 matrix metalloproteinase is associated with cervical carcinoma progression and invasion. *Cancer Res.* **65,** 6543–6550 (2005).
7. Basbaum, C. B. & Werb, Z. Focalized proteolysis: spatial and temporal regulation of extracellular matrix degradation at the cell surface. *Curr. Opin. Cell Biol.* **8,** 731–738 (1996).
8. Egeblad, M. & Werb, Z. New functions for the matrix metalloproteinases in cancer progression. *Nature Rev. Cancer* **2,** 161–174 (2002).
9. Hotary, K., Allen, E., Punturieri, A., Yana, I. & Weiss, S. J. Regulation of cell invasion and morphogenesis in a three-dimensional type I collagen matrix by membrane-type matrix metalloproteinases **1,** 2, and 3. *J. Cell Biol.* **149,** 1309–1323 (2000).
10. Sabeh, F. *et al.* Tumor cell traffic through the extracellular matrix is controlled by the membrane-anchored collagenase MT1-MMP. *J. Cell Biol.* **167,** 769–781 (2004).
11. Uekita, T., Itoh, Y., Yana, I., Ohno, H. & Seiki, M. Cytoplasmic tail-dependent internalization of membrane-type 1 matrix metalloproteinase is important for its invasion-promoting activity. *J. Cell Biol.* **155,** 1345–1356 (2001).
12. Olson, M. W., Gervasi, D. C., Mobashery, S. & Fridman, R. Kinetic analysis of the binding of human matrix metalloproteinase-2 and -9 to tissue inhibitor of metalloproteinase (TIMP)-1 and TIMP-2. *J. Biol. Chem.* **272,** 29975–29983 (1997).
13. Wolf, K. *et al.* Compensation mechanism in tumor cell migration: mesenchymal–amoeboid transition after blocking of pericellular proteolysis. *J. Cell Biol.* **160,** 267–277 (2003).
14. Ellerbroek, S. M., Wu, Y. I., Overall, C. M. & Stack, M. S. Functional interplay between type I collagen and cell surface matrix metalloproteinase activity. *J. Biol. Chem.* **276,** 24833–24842 (2001).
15. Artym, V. V., Zhang, Y., Seillier-Moiseiwitsch, F., Yamada, K. M. & Mueller, S. C. Dynamic interactions of cortactin and membrane type 1 matrix metalloproteinase at invadopodia: defining the stages of invadopodia formation and function. *Cancer Res.* **66,** 3034–3043 (2006).
16. Furmaniak-Kazmierczak, E., Crawley, S. W., Carter, R. L., Maurice, D. H. & Cote, G. P. Formation of extracellular matrix-digesting invadopodia by primary aortic smooth muscle cells. *Circ. Res.* **100,** 1328–1336 (2007).
17. Galvez, B. G., Matias-Roman, S., Yanez-Mo, M., Sanchez-Madrid, F. & Arroyo, A. G. ECM regulates MT1-MMP localization with β1 or αvβ3 integrins at distinct cell compartments modulating its internalization and activity on human endothelial cells. *J. Cell Biol.* **159,** 509–521 (2002).
18. Holmbeck, K. *et al.* MT1-MMP-deficient mice develop dwarfism, osteopenia, arthritis, and connective tissue disease due to inadequate collagen turnover. *Cell* **99,** 81–92 (1999).
19. Hotary, K. B. *et al.* Membrane type I matrix metalloproteinase usurps tumor growth control imposed by the three-dimensional extracellular matrix. *Cell* **114,** 33–45 (2003).
20. Deryugina, E. I., Luo, G. X., Reisfeld, R. A., Bourdon, M. A. & Strongin, A. Tumor cell invasion through matrigel is regulated by activated matrix metalloproteinase-2. *Anticancer Res.* **17,** 3201–3210 (1997).
21. Will, H., Atkinson, S. J., Butler, G. S., Smith, B. & Murphy, G. The soluble catalytic domain of membrane type 1 matrix metalloproteinase cleaves the propeptide of progelatinase A and initiates autoproteolytic activation. Regulation by TIMP-2 and TIMP-3. *J. Biol. Chem.* **271,** 17119–17123 (1996).
22. Yamada, K. M. *et al.* Monoclonal antibody and synthetic peptide inhibitors of human tumor cell migration. *Cancer Res.* **50,** 4485–4496 (1990).
23. Hegerfeldt, Y., Tusch, M., Brocker, E. B. & Friedl, P. Collective cell movement in primary melanoma explants: plasticity of cell–cell interaction, β1-integrin function, and migration strategies. *Cancer Res.* **62,** 2125–2130 (2002).
24. Bell, C. D. & Waizbard, E. Variability of cell size in primary and metastatic human breast carcinoma. *Invasion Metastasis* **6,** 11–20 (1986).
25. Wicki, A. *et al.* Tumor invasion in the absence of epithelial–mesenchymal transition: podoplanin-mediated remodeling of the actin cytoskeleton. *Cancer Cell* **9,** 261–272 (2006).
26. McNiff, J. M., Subtil, A., Cowper, S. E., Lazova, R. & Glusac, E. J. Cellular digital fibromas: distinctive CD34-positive lesions that may mimic dermatofibrosarcoma protuberans. *J. Cutan. Pathol.* **32,** 413–418 (2005).
27. Nabeshima, K. *et al.* Front-cell-specific expression of membrane-type 1 matrix metalloproteinase and gelatinase A during cohort migration of colon carcinoma cells induced by hepatocyte growth factor/scatter factor. *Cancer Res.* **60,** 3364–3369 (2000).
28. Sameni, M., Dosescu, J., Moin, K. & Sloane, B. F. Functional imaging of proteolysis: stromal and inflammatory cells increase tumor proteolysis. *Mol. Imaging* **2,** 159–175 (2003).
29. Bravo-Cordero, J. J. *et al.* MT1-MMP proinvasive activity is regulated by a novel Rab8-dependent exocytic pathway. *EMBO J.* **26,** 1499–1510 (2007).
30. Christiansen, J. J. & Rajasekaran, A. K. Reassessing epithelial to mesenchymal transition as a prerequisite for carcinoma invasion and metastasis. *Cancer Res.* **66,** 8319–8326 (2006).
31. Lauffenburger, D. A. & Horwitz, A. F. Cell migration: a physically integrated molecular process. *Cell* **84,** 359–369 (1996).
32. Ridley, A. J. *et al.* Cell migration: integrating signals from front to back. *Science* **302,** 1704–1709 (2003).
33. Cukierman, E., Pankov, R., Stevens, D. R. & Yamada, K. M. Taking cell–matrix adhesions to the third dimension. *Science* **294,** 1708–1712 (2001).
34. Belkin, A. M. *et al.* Matrix-dependent proteolysis of surface transglutaminase by membrane-type metalloproteinase regulates cancer cell adhesion and locomotion. *J. Biol. Chem.* **276,** 18415–18422 (2001).
35. Wyckoff, J. B., Pinner, S. E., Gschmeissner, S., Condeelis, J. S. & Sahai, E. ROCK- and myosin-dependent matrix deformation enables protease-independent tumor-cell invasion *in vivo*. *Curr. Biol.* **16,** 1515–1523 (2006).
36. Saltel, F., Destaing, O., Bard, F., Eichert, D. & Jurdic, P. Apatite-mediated actin dynamics in resorbing osteoclasts. *Mol. Biol. Cell* **15,** 5231–5241 (2004).
37. Nisato, R. E. *et al.* Dissecting the role of matrix metalloproteinases (MMP) and integrin $\alpha_v\beta3$ in angiogenesis *in vitro*: absence of hemopexin C domain bioactivity, but membrane-type 1-MMP and $\alpha_v\beta3$ are critical. *Cancer Res.* **65,** 9377–9387 (2005).
38. Tam, E. M., Wu, Y. I., Butler, G. S., Stack, M. S. & Overall, C. M. Collagen binding properties of the membrane type-1 matrix metalloproteinase (MT1-MMP) hemopexin C domain. The ectodomain of the 44-kDa autocatalytic product of MT1-MMP inhibits cell invasion by disrupting native type I collagen cleavage. *J. Biol. Chem.* **277,** 39005–39014 (2002).
39. Chen, W. T. & Wang, J. Y. Specialized surface protrusions of invasive cells, invadopodia and lamellipodia, have differential MT1-MMP, MMP-2, and TIMP-2 localization. *Ann. NY Acad. Sci.* **878,** 361–371 (1999).
40. Filla, M. B. *et al.* Dynamic imaging of cell, extracellular matrix, and tissue movements during avian vertebral axis patterning. *Birth Defects Res. C Embryo Today* **72,** 267–276 (2004).
41. Petroll, W. M., Cavanagh, H. D. & Jester, J. V. Dynamic three-dimensional visualization of collagen matrix remodeling and cytoskeletal organization in living corneal fibroblasts. *Scanning* **26,** 1–10 (2004).
42. Takino, T. *et al.* Membrane-type 1 matrix metalloproteinase modulates focal adhesion stability and cell migration. *Exp. Cell Res.* **312,** 1381–1389 (2006).
43. Wolf, K., Muller, R., Borgmann, S., Brocker, E. B. & Friedl, P. Amoeboid shape change and contact guidance: T-lymphocyte crawling through fibrillar collagen is independent of matrix remodeling by MMPs and other proteases. *Blood* **102,** 3262–3269 (2003).
44. Sahai, E. & Marshall, C. J. Differing modes of tumour cell invasion have distinct requirements for Rho/ROCK signalling and extracellular proteolysis. *Nature Cell Biol.* **5,** 711–719 (2003).
45. Zaman, M. H. *et al.* Migration of tumor cells in 3D matrices is governed by matrix stiffness along with cell–matrix adhesion and proteolysis. *Proc. Natl Acad. Sci. USA* **103,** 10889–10894 (2006).
46. Haas, P. & Gilmour, D. Chemokine signaling mediates self-organizing tissue migration in the zebrafish lateral line. *Dev. Cell* **10,** 673–680 (2006).
47. Sympson, C. J. *et al.* Targeted expression of stromelysin-1 in mammary gland provides evidence for a role of proteinases in branching morphogenesis and the requirement for an intact basement membrane for tissue-specific gene expression. *J. Cell Biol.* **125,** 681–693 (1994).
48. Hiraoka, N., Allen, E., Apel, I. J., Gyetko, M. R. & Weiss, S. J. Matrix metalloproteinases regulate neovascularization by acting as pericellular fibrinolysins. *Cell* **95,** 365–377 (1998).
49. Billinghurst, R. C. *et al.* Enhanced cleavage of type II collagen by collagenases in osteoarthritic articular cartilage. *J. Clin. Invest.* **99,** 1534–1545 (1997).

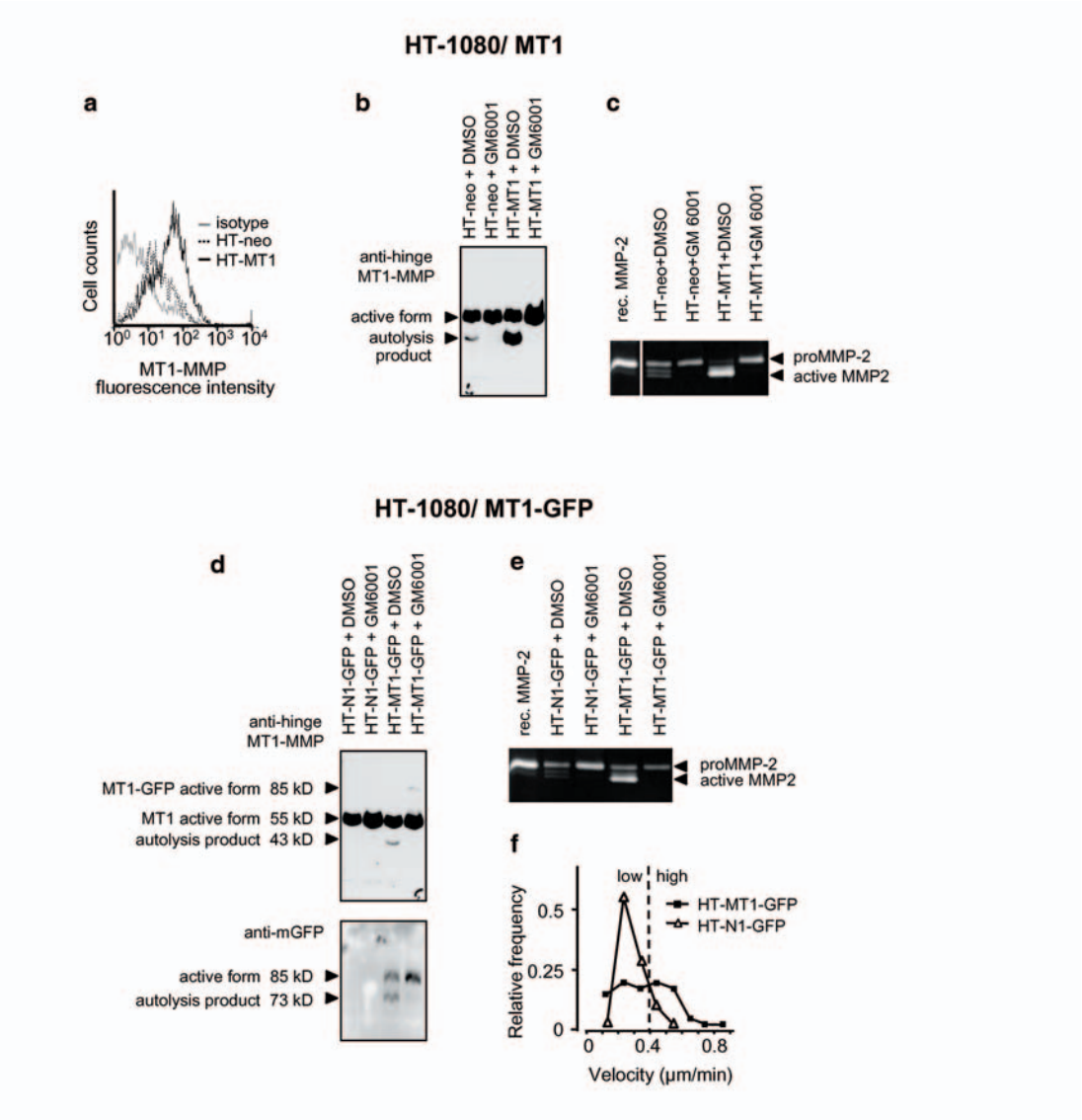

Figure S1. Increased surface level and activation state of MT1-MMP and MMP-2 in HT-1080 cells after transfection with MT1-MMP or MT1-MMP-GFP. Overexpression of MT1-MMP leads to increased MT1-MMP autolysis and MMP-2 activation, confirming its active state. (a) Increased MT1-MMP cell-surface expression as detected by flow cytometry (Ab 815). (b) Increased autolysis of cell-surface MT1-MMP after transfection, using surface biotinylation, protein capture by streptavidin-conjugated beads and detection by Western blot (Ab 815). The accumulation of the active form resulted from treatment with MMP-inhibitor GM6001. (c) MMP-2 gelatinolytic activity from cell lysates detected by gelatin zymography. Increased MMP-2 activation was induced by overexpressing MT1-MMP and reverted by MMP inhibitor GM6001. (d) Cell-surface localized MT1-MMP and MT1-MMP-GFP surface expression in cells transfected with N1-GFP control or MT1-MMP-GFP vector. Cell-surface proteins were analysed by Western blot. Anti-hinge MT1-MMP Ab (Ab815) was used to detect total MT1-MMP (upper panel) and anti-monomeric GFP (mGFP) mAb (clone JL-8; Clontech) to detect MT1-GFP fusion protein (lower panel). Cell-surface MT1-MMP-GFP (lower panel) represented a minor fraction, compared to endogenous MT1-MMP. Increased MT1-MMP activation and processing after expression of MT1-MMP-GFP was confirmed by the appearance of the 43 kD autoloysis product (upper panel). (e) Increased MMP-2 activation after expression of MT1-MMP-GFP but not N1-GFP control vector, detected by gelatin zymography. MMP-2 activation was reverted by MMP inhibitor GM6001. (f) Increase of high velocity subset in HT-1080 cells after expression of MT1-MMP-GFP, similar to expression of wtMT1-MMP depicted in Fig. 1d (40 cells; **, P=0,0094, unpaired Mann-Whitney *U*-test). Correct surface localization and functionality of MT1-MMP-GFP was confirmed for MDA-MB-231 breast carcinoma cells (not shown). For confocal microscopy, cells with low GFP expression level that additionally lacked bright signal from intracellular vesicles or endoplasmic reticulum were selected.

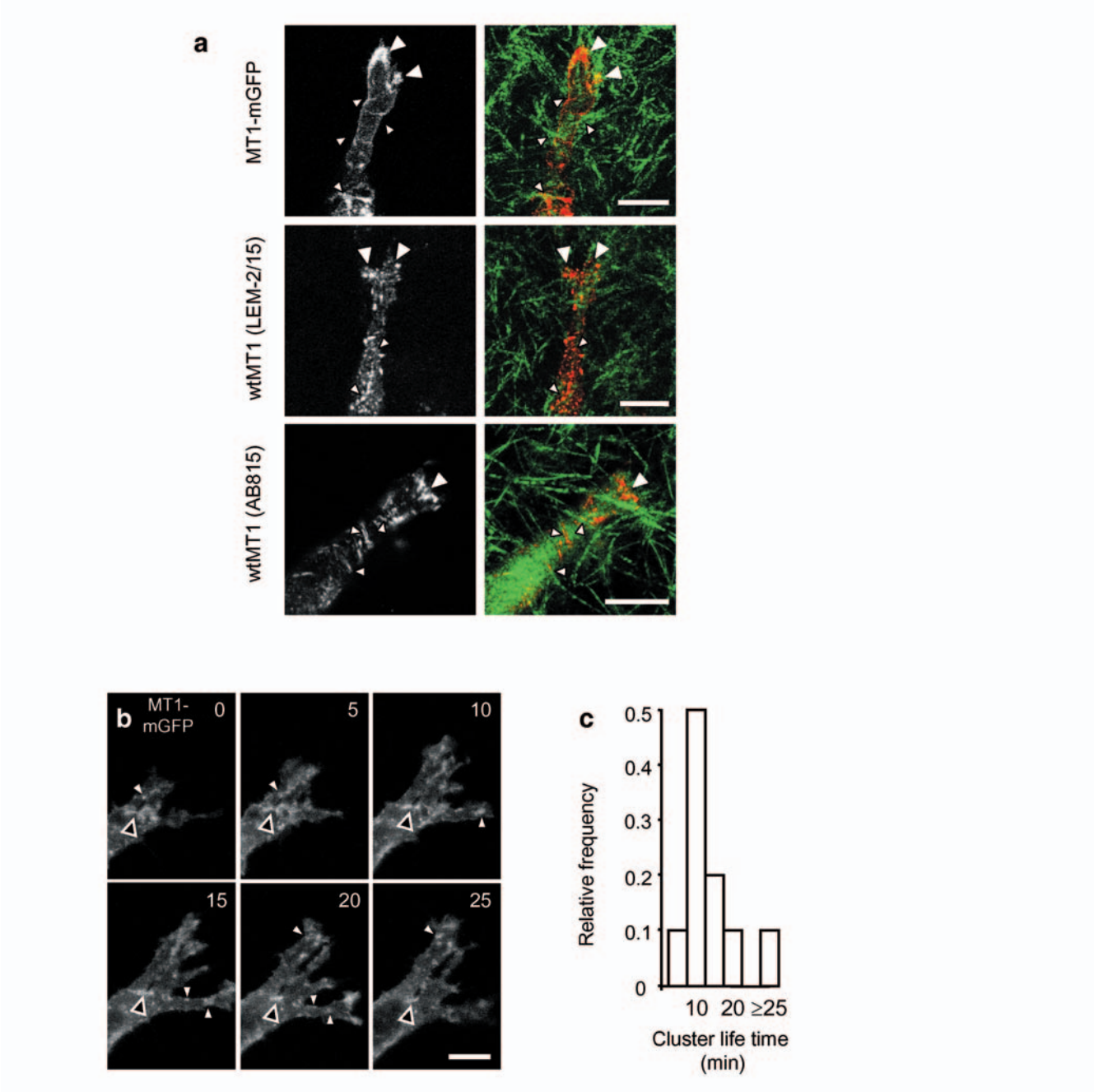

Figure S2. Topography and dynamics of MT1-MMP focalization in HT-1080 cells. (a) Equivalent focalization of MT1-MMP-mGFP and wtMT1-MMP detected by Abs AB815 and LEM-2/15 (red) at cell interactions to collagen fibres (green; confocal reflection). All three detection protocols yielded the same enrichment of MT1-MMP at leading tips (large arrowheads) and focal to belt-like clustering along perpendicular fibres crossing the cell surface (small arrowheads). (b) Dynamic formation and disappearance of MT1-MMP-rich clusters at the leading edge generating force towards collagen fibres. Short- and longer-lived MT1-MMP focalization occurred predominantly in contact zones to collagen fibres (see two-channel sequence in Supplementary Information, movie 1). MT1-MMP-mGFP-expressing HT-1080 cell migrating in 3D collagen was monitored for 30 min by serial z-scanning. White arrowheads, short-lived MT1-MMP-GFP clusters at collagen fibres. Black arrowhead, more stable focalization of MT1-MMP-GFP at Y-type fibre insertion between 2 pseudopod branches. (c) Frequency distribution of MT1-MMP-GFP cluster life-time, derived from the sequence depicted in (b). Similar short- and long-lived cluster life-time was confirmed for MDA-MB-231 cells expressing MT1-MMP-GFP (not shown). Bars, 10 μm.

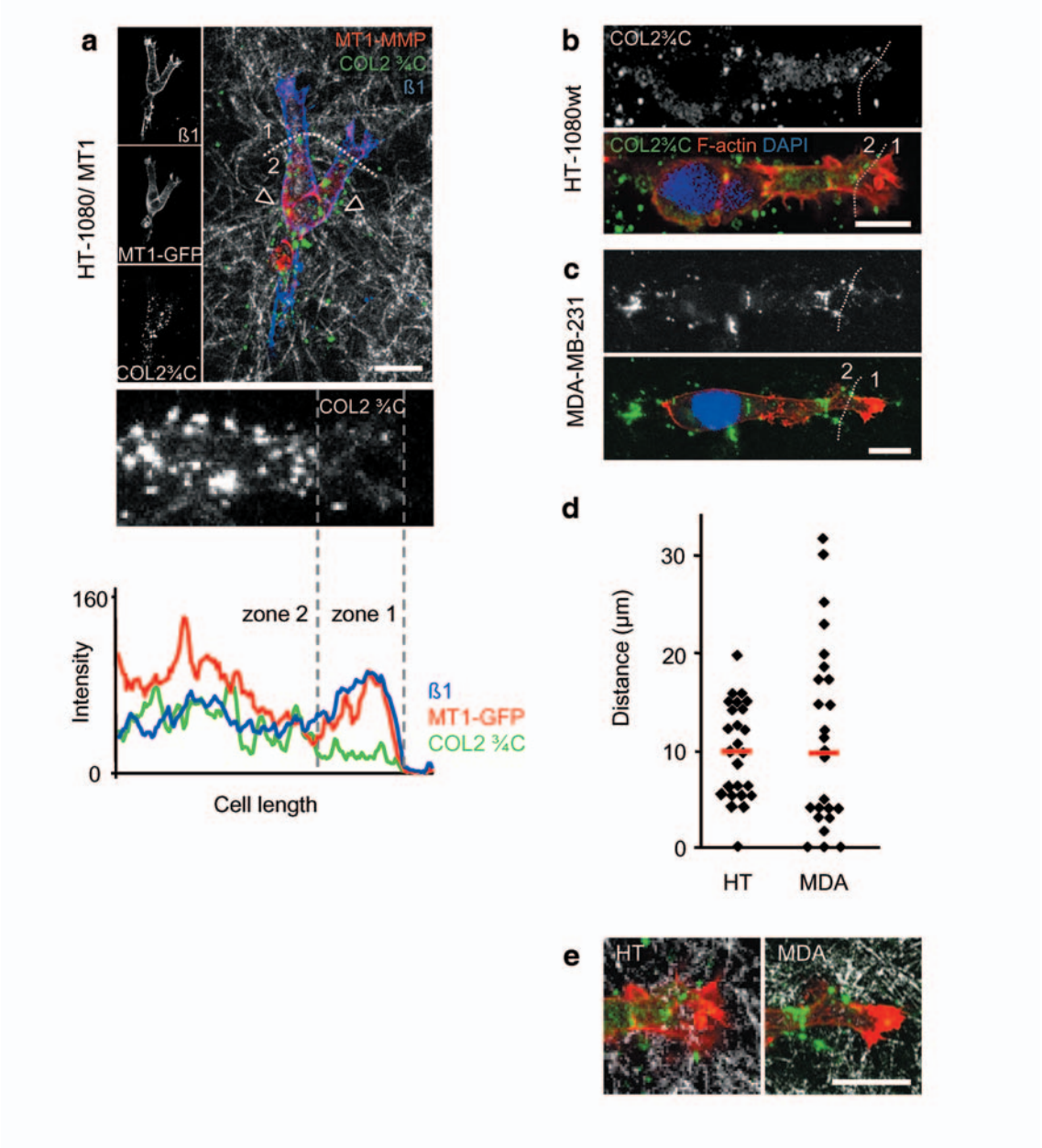

Figure S3. Segregation into anterior adhesion (zone 1) and posterior collagenolytic compartment (zone 2) in HT-MT1 (a), HT-1080wt (b) and MDA-MBA-231wt (c) cells. Localization of ß1 integrins (blue), MT1-MMP-mGFP or F-actin (red) and COL2¾C$_{short}$ epitope (green) (a-c, e). (d) Distance between anterior actin-rich pseudopod ruffle and the first posterior peak of COL2¾Cshort epitope (medians from 25 cells of 3 independent experiments). (e) Interaction of anterior actin-rich pseudopods (red) with collagen fibres, lacking COL2¾Cshort epitope (green). Black arrowheads, selected perpendicular collagen fibres. Bars, 10 µm.

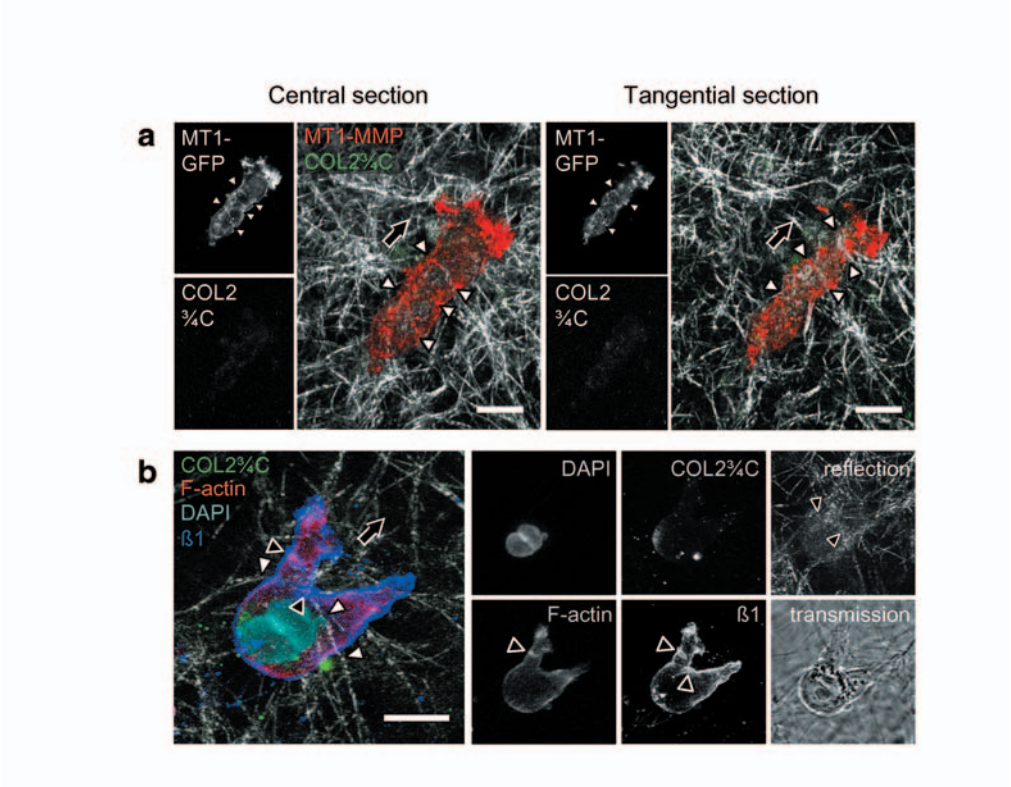

Figure S4. PI treatment prevents collagenolysis but not the focalization of MT1-MMP, ß1 integrin, and F-actin at binding sites to perpendicular collagen fibres in HT-MT1 cells. (a) MT1-MMP (red), reflection (grey) and COL2¾C$_{short}$ epitope (green) from a central (left) and tangential (right) section. (b) Colocalization of F-actin (red), ß1 integrins (blue), COL2¾C$_{short}$ epitope (green) and DAPI (cyan) at fibre-binding sites in the presence of PI. White arrowheads, perpendicular collagen fibres; black arrowheads, regions of colocalization. Bars, 10 µm.

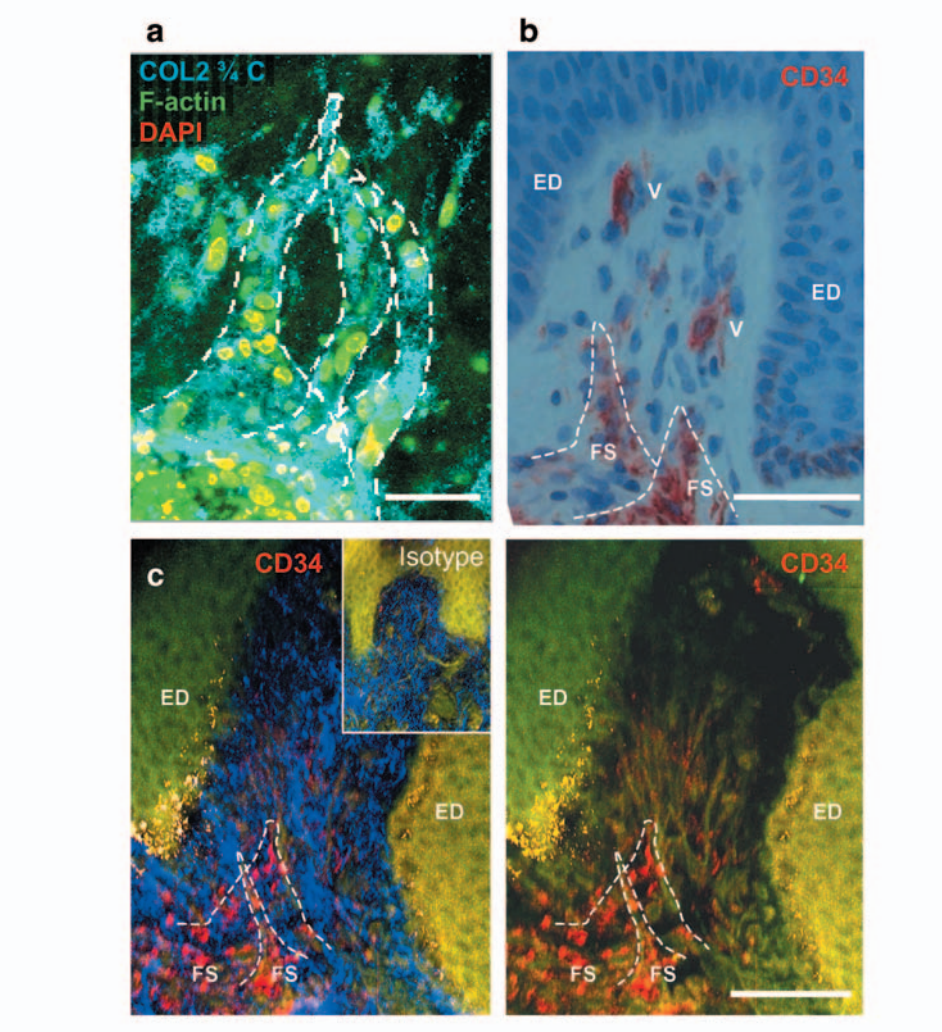

Figure S5. In vitro-in vivo comparison of fibrosarcoma invasion pattern. (a) Invasive cell strands obtained from HT-MT1 cells in 3D spheroid assay in 3D collagen in vitro. Staining of cells with Calcein (green), DAPI (red) and COL2¾C$_{short}$ epitope (cyan). The calibre of invasive strands as well as strand convergence mimic fibrosarcoma invasion and growth pattern in vivo (b-c). (b-c) Multicellular invasion pattern at the margin of a human primary lesion of a dermatofibrosarcoma protuberans adjacent to the epidermis. CD34 was used as a marker to discriminate fibrosarcoma (and endothelial) cells from the surrounding stroma. FS, fibrosarcoma; ED, epidermis; V, vessel. (b) Paraffin-embedded section stained with hematoxilin-eosin (blue) and anti-CD34 mAb (red; immunoperoxidase reaction; LSAB^{TM+}/HRP detection kit; DAKO). (c) PFA-fixed cryosections stained with anti-mouse CD34 mAb or isotypic control (red), monitored by multiphoton-excited fluorescence together with second harmonic generation of collagen fibrils (blue). Green and red autofluorescence emission was most prominent in the epidermis, dermal elastic fibres and ducts from dermal glands. 3D projections from z-stacks representing 18 µm depth. Bars, 50 µm.

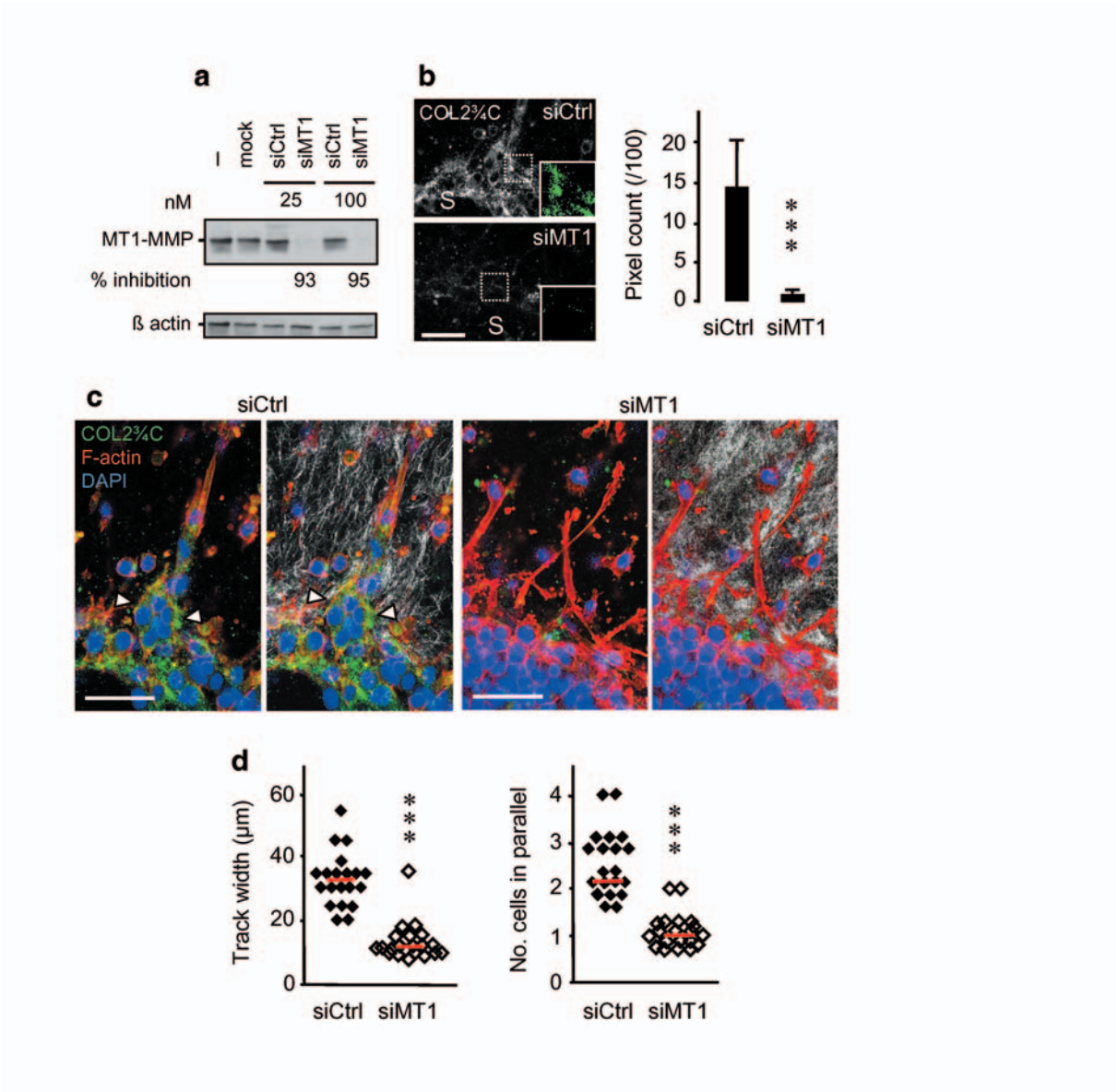

Figure S6. Inhibition of collagenolysis, track formation and multicellular invasion by MT1-MMP knockdown in HT-1080 wild-type cells. (a) Efficiency of MT1-MMP knockdown by RNAi determined by Western blot and normalisation to ß-actin content (66-93% for 25 nM and 75-95% for 100 nM siMT1; n=3). (b) Reduced collagenolysis surrounding the spheroid after 20h of culture in 3D collagen lattice (3.3 mg/ml), as detected by the COL2¾C$_{short}$ epitope (left). Subtotal inhibition of collagenolysis was quantified from tresholded images (insets) and analysed for mean pixel intensities ± SD (n=3; p<0.0001, unpaired one-tailed Student's t test). (c) Abrogation of collagenolytic track formation and multicellular invasion (left) towards individually invading cells by RNAi against MT1-MMP (right). (d) Reduction of track width and number of cells in parallel after knockdown of MT1-MMP (p<0.0001, Mann-Whitney *U*-test).

Supplementary Movies

Supplementary Movie 1. Localization dynamics of MT1-MMP-GFP in HT-1080 cell moving in 3D collagen lattice. The movie shows the cell depicted in Supplementary Information, Fig. S2b. Short-lived MT1-MMP-mGFP clusters form and resolve at pseudopods within 5-15 min, whereas pseudopod binding to collagen fibrils persists for longer time periods (white arrowheads). A singular long-lived cluster persists for 25 min and longer at Y-type fibre inserting between pseudopod branches (black arrowhead). Maximum intensity projection of time-lapse confocal z-stack at 5 min time intervals. Field size: 80x80 μm.

Supplementary Movie 2. Localization dynamics of HT-MT1 cell-mediated collagen fibre cleavage and dislocation. The sequence corresponds to Fig. 3d-e. Dynamic changes of (a) cell morphology and collagen fibres, (b) ^{DQ}FITC signal and cell outline, (c) ^{DQ}FITC signal and transmission and (d) summarizing scheme highlighting the opening of fibre belts and transport of loose ends. Arrowheads: location of diameter expansion of the cell body (b); fibre bending in forward direction, associated with nuclear movement (c); protruding pseudopods that lack ^{DQ}FITC signal (d). Asterisk in (b) shows proteolytic path present after cell rear retration. Maximum intensity projection of simultaneous 4-channel time-lapse movie from z-stack taken at 5 min intervals. Field size: 65x65 μm.

Supplementary Movie 3. Persistent migration at decreased rates after inhibition of pericellular proteolysis within high-density collagen matrices (10 mg/ml). The movie corresponds to Fig. 5b. HT-MT1 cells invading from a spheroid in the absence or presence of PI cocktail. Time-lapse bright-field microscopy during 5 h of observation. Field size: 300x500 μm.

Supplementary Movie 4. Transition from individual to collective invasion pattern. (a) Extensive tube-like matrix defects (detected by the loss of grey reflection signal) bordered by COL2¾C$_{short}$ epitope (green) were created by single HT-MT1 cells moving in single-cell chains. White arrowheads, entire track; intermittent black arrowheads, focal plane of the matrix defect. Movie shows the z-stack corresponding to Fig. 6c. (b) Conversion from individual to collective invasion strands along regions of proteolytically remodeled collagen matrix. Three independent strands converge to a complex strand pattern (arrowheads). Movie shows the z-stack corresponding to Fig. 6d. (c) Rotation of central section from (b). Calcein-labeled cells (green), nuclei (red) and COL2¾C$_{short}$ epitope (cyan). Z-scans were taken at 2 μm intervals for a total depth of 28 (a), 22 (b) and 16 μm (c). Field size: 375x375 μm (a,b).

Supplementary Movie 5. Colocalization of MT1-MMP and collagen degradation along emerging multicellular invasion strand of HT-MT1 cells. Z-stack and rotation correspond to Fig. 6e-g. (a) Colocalization (arrowheads) of MT1-MMP (LEM 2/15; red) with COL2¾C$_{short}$ epitope (green) along the near-continuous circular cell-matrix interface (grey). Z-scans represent 54 μm of depth. Field size: 134x134 μm. (b) Rotation of the same invasion zone, confirming the continuous, layer-type cell-matrix interface.

Supplementary Movie 6. Abrogation of multicellular invasion pattern by protease inhibitor (PI) cocktail. Z-stacks correspond to Fig. 7a. Transition to multicellular strands (arrowheads, left) was abrogated by PI, yet protease-independent single cell migration persisted (right). Z-scans represent 14 μm of depth. Field size: 375x375 μm.

Supplementary Methods

Flow cytometry

For flow cytometry of surface MT1-MMP, cells were released from the collagen lattice by highly purified collagenase type VII from *Clostridium histolyticum* (Sigma), stained with MT1-MMP antibody (Ab815, Chemicon) and secondary Alexa488-conjugated anti-rabbit IgG and analyzed.

Detection of cell surface proteins expression and enzymatic activity

Labeling of cell surface proteins was performed as described[1]. Cells were cultured overnight with or without GM6001 (25 μM) (Chemicon), washed with PBS and incubated with Sulfo-6-[(+)-Biotinamidocaproylamido]caproic acid N-hydroxysuccinimide ester (Biotin-LC-LC-NHS; Pierce) for 10 min on ice, washed with glycine (100 mM) to quench remaining NHS groups and dissolved in lysis buffer. Surface proteins were precipitated by incubation with NeutrAvidin-conjugated beads (Pierce) for 1 h, eluted by boiling in SDS sample dilution buffer for 15 min, separated by gel electrophoresis and detected by Western blot. After surface protein precipitation, the gelatinolytic activity of MMP-2 was detected by zymography within gelatin-containing acrylamid gels[2].

Multiphoton microscopy of human fibrosarcoma samples

Frozen sections of human dermatofibrosarcoma protuberans samples were fixed with PFA and stained with mouse monoclonal anti-CD34 IgG_1 (clone QBEnd-10; DAKO) or isotypic control IgG_1 and Alexa546-conjugated anti-mouse IgG and monitored by multiphoton microscopy. Multiphoton microscopy using a 20x water NA 0.95 objective was carried out on an Olympus microscope equipped with a single-beam scan head and 4 non-descanned photomultipliers in each forward and backward direction (LaVision Biotec) coupled to a pulsed Chameleon-XR laser (Coherent). Excitation wavelength was 850 nm, emission was

collected at 420/20 nm (second harmonic generation of collagen structures), 510/30 nm (green autofluorescence) and 590/50 nm (red fluorescence).

MT1-MMP-GFP and N1-GFP vector generation

A fusion protein of monomeric (m)GFP tagged to the c-terminus of human MT1-MMP was generated. The pEGFP-N1 vector (Clontech) was modified by introducing a A206K mutation at the GFP segment to prevent low-affinity-GFP aggregation[3] and used for subsequent cloning. The cDNA of human MT1-MMP was kindly provided by Dr. D. Pei (University of Minnesota, Minneapolis, MN). The MT1-MMP-monomeric (m)GFP expression construct was generated by shuttling the MT1-MMP open reading frame into the modified pEGFP-N1 vector using the NheI and SacII site, tagging mGFP via a linker segment (PRARDPPVAT) to the C-terminal site of MT1-MMP. The PCR reactions were performed with high-fidelity Pfu polymerase (Stratagene). The plasmid sequence was verified by DNA sequencing before transfection and generation of stable cell lines.

References

1. Munshi, H.G., Wu, Y.I., Ariztia, E.V. & Stack, M.S. Calcium regulation of matrix metalloproteinase-mediated migration in oral squamous cell carcinoma cells. *J Biol Chem* **277**, 41480-8 (2002).
2. Ellerbroek, S.M., Wu, Y.I., Overall, C.M. & Stack, M.S. Functional interplay between type I collagen and cell surface matrix metalloproteinase activity. *J Biol Chem* **276**, 24833-42 (2001).
3. Zacharias, D.A., Violin, J.D., Newton, A.C. & Tsien, R.Y. Partitioning of lipid-modified monomeric GFPs into membrane microdomains of live cells. *Science* **296**, 913-6 (2002).